6-2015

The Design of an Optimized Patient-Specific In Vivo Spinal Fusion Cage Using Additive Manufacturing

Gorman Donnelly
Union College - Schenectady, NY

Department of Mechanical Engineering at Union College
Senior Project Report for the Winter of 2015

THE DESIGN OF AN OPTIMIZED PATIENT-SPECIFIC IN VIVO SPINAL FUSION CAGE USING ADDITIVE MANUFACTURING

Student:

Gorman Donnelly

March 17, 2015

Academic Terms:

Fall '14, Winter '15

Committed Faculty Member:

Glenn Sanders, Ph. D.

TABLE OF CONTENTS

I. ABSTRACT

This project involved the design of an all-in-one patient-specific lumbar spinal fusion cage using Direct Metal Laser Sintering (DMLS) manufacturing. The cage is zero-profile and does not need the use of supplemental fixation. It was manufactured out of the titanium alloy Ti-6Al-4V using a DMLS rapid prototyping machine from a third party company. The endplates of the cage are patient-specific allowing for a larger surface contact area between the cage and the vertebral bodies than most cages on the market. This fosters a more successful fusion as well as decreases surgery time, effectively decreasing recovery time. Different porosity variations of the design were tested and optimized by conducting a comprehensive analysis on a representative volume element (RVE). The RVE consisted of a one cubic centimeter cube with a non-uniform porosity. The results of the RVE analysis were then applied to the cage porosity. The purpose of optimizing the pores was to achieve an effective modulus of elasticity of approximately the same magnitude of bone (1.5 GPa) as well as to foster bone growth between the bone graft and the vertebral endplates. The final design has an effective modulus of 2.576 GPa and a porosity of 69.939%.

II. BACKGROUND INFORMATION

II.i Spine:

The lumbar spine refers to the lower back and is made up of five vertebral bodies labeled L1-L5 and support the weight of the entire torso. In between each vertebral body lies an intervertebral disc made of a thick outer layer (the annulus) surrounding a gel-like center (nucleus). The intervertebral discs act as shock absorbers for the spine and help support the compressive forces of a person's body weight.[1] It has been shown that the compressive force

experienced by the discs can increase from 200 percent to 300 percent of the person's body weight depending on the activity that they are doing.[2] The spine has three fundamental biomechanical functions: (1) to guarantee the load transfer along the spinal column without instability, (2) to allow sufficient physiologic mobility and flexibility, and (3) to protect the delicate spinal cord from damaging forces and motions.[3] The lumbar spine experiences the largest loading out of the entire spine and is also responsible for lower spinal mobility. Therefore it is imperative that the lumbar fusion cage facilitates bone growth that can fulfill the role of a lumbar intervertebral disc effectively and efficiently.

II.ii Diseased Spine:

Spinal fusion is a surgical process that is often used to resolve problems with the intervertebral discs in the spine. This process has proven successful in relieving symptoms for patients experiencing Degenerative Disc disease, Spondylolisthesis (displacement of a vertebra), fracture, or cancerous tumors.[4] One of the most common cases that require spinal fusion is disc degeneration. When the disc degenerates, the deformed disc and the vertebral bodies surrounding it can often pinch nerves emanating from the spinal cord causing discomfort and pain. This can be seen in Figure 1 below.

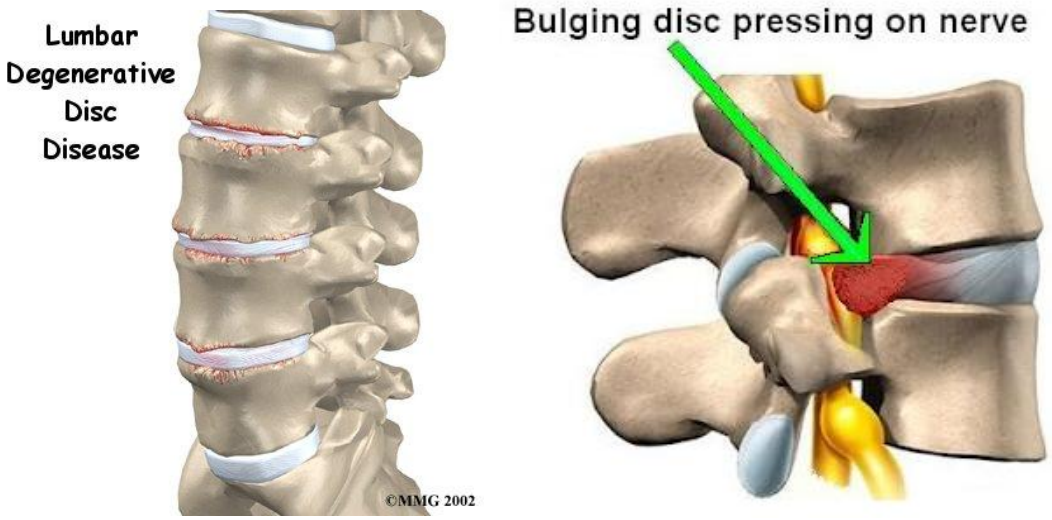

Figure 1: Degenerative disc disease (left) and disc bulging (right) are examples of a diseased spine.[1]

Many patients improve with conservative treatment such as physical therapy. Otherwise, surgeons then perform a spinal fusion by removing the degenerating disc and replacing it with a cage filled with bone graft most often taken from the patient's iliac crest.[5] This process allows osseointegration to occur so that bone grows through the cage, essentially "welding" the two unstable vertebrae together into one stable bone as shown in Figure 2 below.

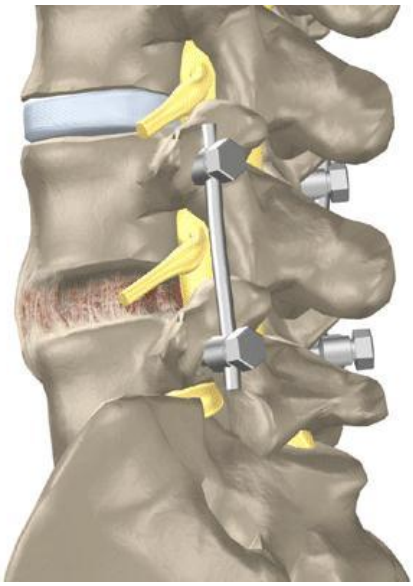

Figure 2: Successful bone fusion in disc space between two vertebral bodies causing the pain.[6]

II.iii Spinal Fusion Surgery:

A spinal fusion surgery is designed to "stop the motion at a painful vertebral segment, which in turn should decrease pain generated from the joint".[1] Therefore, it is an inherent part of the surgery that the patient will lose some degree of motion, although if only one level of lumbar vertebral bodies is affected then it most likely would not be noticeable. Another possible consequence of the surgery is the possible diagnosis of Adjacent Segment Disease (ASD) where the patient experiences new symptoms that they had not had before. This could refer to experiencing pain in a new location or neurological symptoms.

There are many types of surgery approaches for a lumbar fusion including but not limited to Posterior Lumbar Interbody Fusion (PLIF), Anterior Lumbar Interbody Fusion (ALIF), Transforaminal Lumbar Interbody Fusion (TLIF), and Extreme Lateral Interbody Fusion (XLIF). PLIF is approached from the back while ALIF is done from the front of the patient to remove the injured disc and replace it with the fusion cage stuffed with bone graft. These are two of the most common surgical approaches, however both have their limitations. When approaching the surgery from the back, the surgeon must be careful not to damage the fragile spinal cord that is protected by the vertebrae. Figure 3 displays a simulated replication of a PLIF procedure.

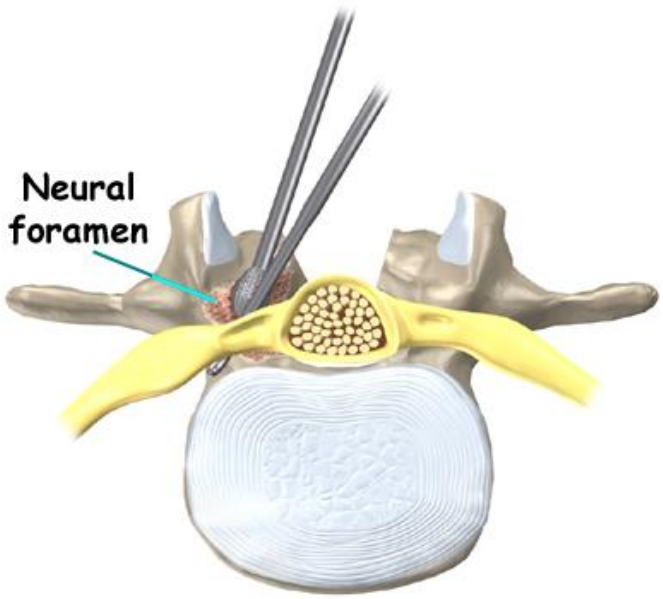

Figure 3: Superior view of a PLIF procedure.[7]

The spinal column and nerves (shown in yellow) must be avoided to keep from damaging or pinching the nerve roots. When approaching from the front, the surgeon must avoid damaging internal organs while attempting to gain entry to the spine.

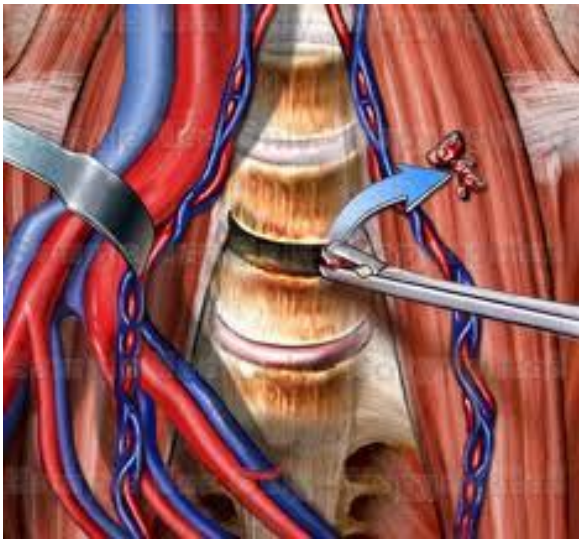

Figure 4: Anterior view of an ALIF procedure.[8]

When approaching from the abdomen, the surgeon must also take great care to avoid damaging the blood vessels (shown in blue and red). Another type of fusion surgery is Transforaminal Lumbar Interbody Fusion (TLIF). TLIF approaches the surgery from the posterior, similar to a PLIF fusion. A TLIF procedure allows the surgeon to insert a cage containing bone graft without needing to move the nerve roots as much as in a PLIF.

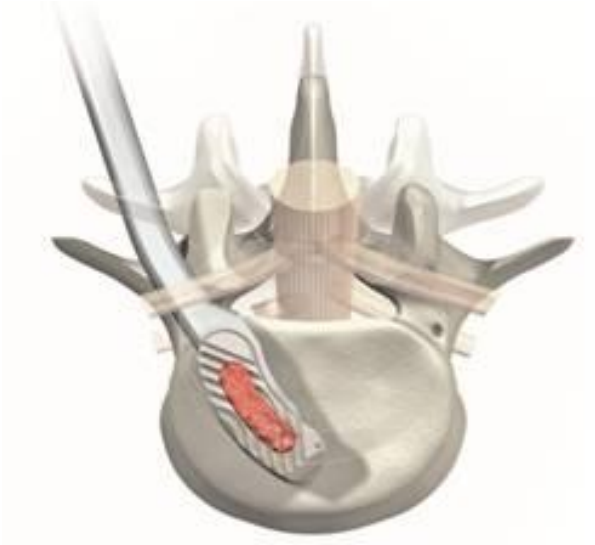

Figure 5: Superior view of a TLIF procedure.[9]

The final type of lumbar spinal fusion is Extreme Lateral Interbody Fusion (XLIF). In this procedure the surgeon accesses the disc space from the side of the patient as opposed to the anterior or posterior.

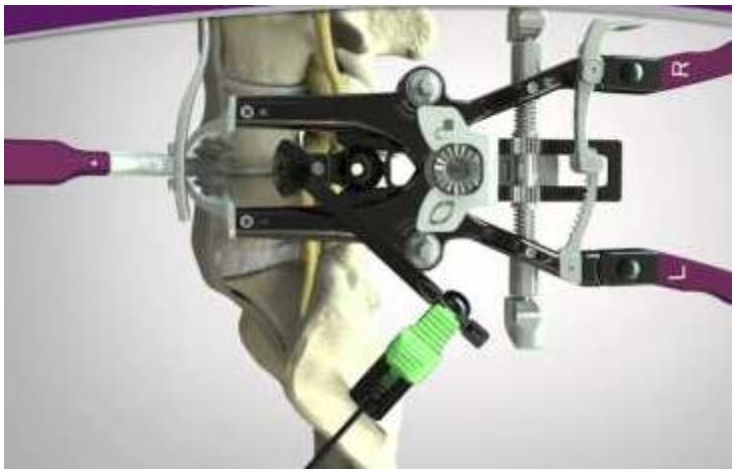

Figure 6: Lateral view of an XLIF procedure.[10]

Each fusion cage is designed with the type of surgery in mind and therefore can only be implanted using the associated approach.

II.iv Fusion Cage Background:

With an ALIF procedure, the cage is sometimes accompanied by a metal plate that is screwed into the two vertebral bodies to maintain stability while the new bone grows. One major limitation with this type of procedure is that implanting the plate increases surgical time, requires additional hardware, and the surgeon is required to enter through the anterior. If fusion is required in the cervical vertebrae, the plate can also cause a patient to experience dysphagia if the plate irritates the throat. Dysphagia is the symptom where patient's experience difficulty swallowing with the sensation that there is something stuck in their throat.

The effectiveness of the procedure depends on the structural integrity, mechanical properties, and graft space of the cage. Lumbar fusion cages most commonly seen in the medical field today are mainly solid structures with a space for bone graft in the middle. A commonly used lumbar cage is shown below in Figure 7. The top and bottom faces of the cage make contact

with the endplates of the adjacent vertebral bodies and it has been designed with ridges to restrain the cage from migrating and foster a solid contact with the endplates. The holes labeled "instrument attachment" are for the instruments that are used by the surgeon to implant the cage into the patient.

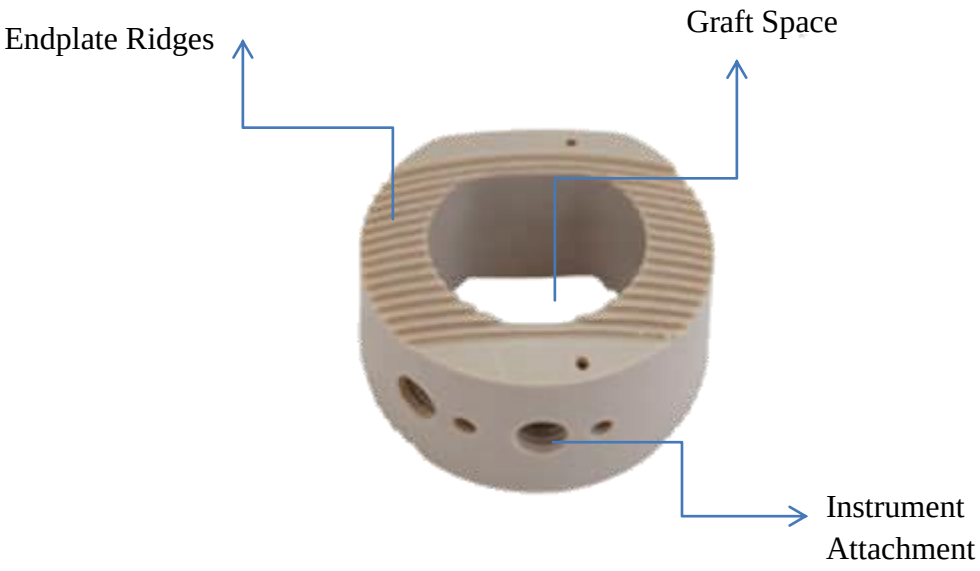

Figure 7: Redondo™ Anterior Lumbar Interbody Fusion Cage.[11]

The cage shown here is made out of PEEK polymer which is a thermoplastic commonly used in medical implants due to its high wear resistance, mechanical strength, and dimensional stability.[12] PEEK is also often used for cages due to its low modulus of approximately 4-24 GPa.[13] There are a variety of types of fusion cage fixations such as cages with a supplemental plate, cages with pedicle rods, and "all-in-one" cages. Images of the cages are shown below in Figure 8 in the order they were mentioned.

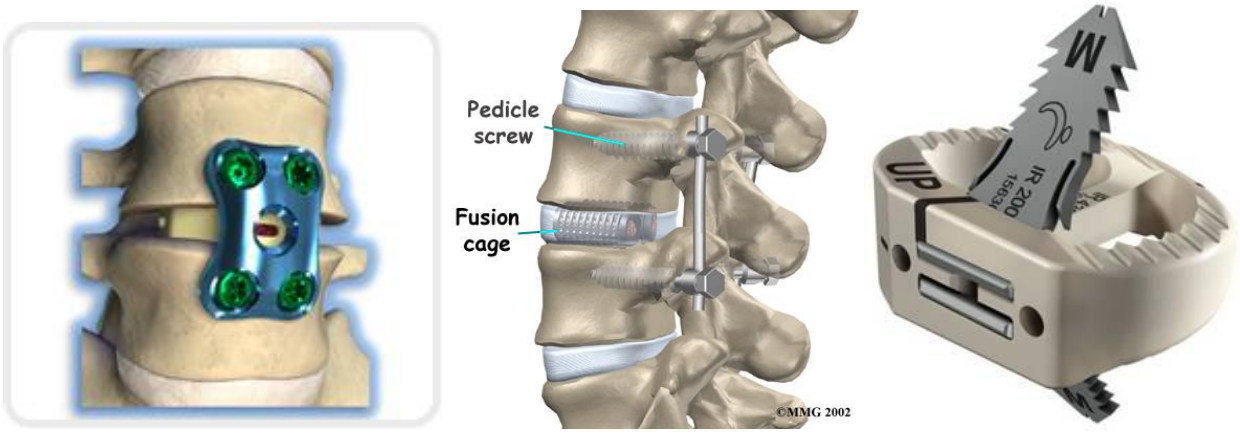

Figure 8: A) Fusion cages with plate,[14] B) with pedicle rods,[15] and C) an all-in-one cage.[16]

The surgery to implant fusion cages that require a plate or pedicle screws typically lengthen the surgery time due to the amount of hardware involved. In terms of the pedicle rods, the surgeon typically has to bend the rod to the specific patient's geometry during surgery which can weaken the material and still may not reflect the optimal geometry for the patient. The all-in-one cage offers a fixation without the need for supplemental hardware. The "blades" of the cage shown on the right in Figure 8 provide the stability that the plate or rods would while remaining entirely within the profile of the removed disc. All-in-one cages may also be affixed to the vertebrae using bone screws.

Titanium is another common material used for the cage body due to its well established material properties and excellent biocompatibility. The cage currently being designed will be manufactured out of the titanium alloy Ti-6Al-4V. Since the majority of a typical cage is solid, the surface area where bone cells are able to grow is limited. This is not ideal because it limits the amount of bone that is able to grow, as well as the speed at which it can grow. There are few cages out there that have begun to solve this problem through the use of increased porosity of the cage structure. Cage porosity creates a much larger surface area for the bone cells to attach to

and grow. This project focuses on optimizing the porosity of a lumbar spinal fusion implant while adhering to structural criteria defined in section III of this report.

II.v Motivation for Patient Specific Design:

Every person's body is unique and it is a vast oversight to assume that they can all be treated the same way. The majority of the cages currently in use today are designed (albeit with a variety of sizes) to be used for any patient. To account for this, the surgeon then has to alter the geometry of the patient's vertebral body endplates during surgery to make the chosen cage fit more effectively. If pedicle rods are used, they must be bent by the surgeon to match the spinal geometry of the patient as close as possible, all during the surgery. The motivation, therefore, to design a patient-specific lumbar fusion cage is to eliminate all of these unneeded procedures that increase surgery time and are not optimal for the patient. It would also allow for improved contact area, leading to an improved distribution of forces, which further will lead to faster healing times. A fusion cage designed to fit the specific patient's endplate geometry would decrease surgery time, foster a stronger and quicker bone growth, and would require few to none supplemental hardware or instrumentation to implant.

The term "patient-specific" refers to the nature of the unique geometry of the implant. Traditionally, fusion cages come in a variety of sizes and the surgeon must pick the size most appropriate to the patient's geometry. He must then alter the geometry of the patient's vertebral bodies themselves to maximize the surface area contact between the implant and the bone. This process is not ideal because it increases the amount of surgery time leaving the patient more prone to infection and the surface contact may still not be optimal.[18] When implanting cages that are not patient-specific the surgeon must use a tool to essentially 'shave" away portions of

the vertebral bodies to increase the amount of contact area between the cage and the body. Maintaining maximum surface contact is important to avoid cage subsidence, where due to the stress concentrations at locations on the cage it will begin to subside into the vertebral body itself. To achieve a successful fusion it is important to maintain the original disc height to avoid reverting back to the original pain that provoked the surgery. When a cage subsides into the bone that disc height is decreased below optimal levels. The degree of subsidence is "inversely proportional to the surface area of contact between the bone graft and the [vertebral body]".[18] Figure 9 below is an image of subsidence in a patient's PLIF fusion one year post-operative.

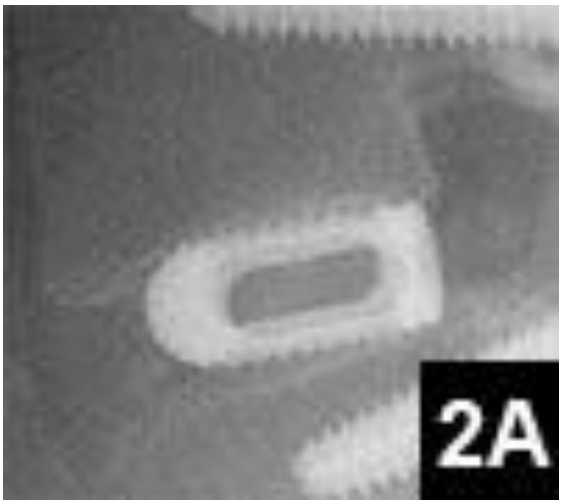

Figure 9: PLIF cage subsidence one year post-operative.[19]

Due to poor surface contact between the cage and the endplates of the vertebral bodies, a good union was not formed between the bone graft and the endplates. Using a specific patient's geometry, the cage can be altered to perfectly match the vertebral bodies to assure optimal surface contact. To accomplish this, a CT scan of the patient's spine is taken and converted into 3D CAD software such as SolidWorks. The location of the diseased level of the spine can then be isolated and the cage can be designed to replace the disc at this location.

The common methodology used when designing these cages is to ensure that physiological stresses remain below the endurance limit of the material (PEEK, titanium, etc.) and to have an effective modulus of elasticity approximately equal to bone (10-20 GPa).[3] Using rigid fixation and this modulus, these cages aim to foster primary bone healing which involves a "direct attempt by the cortex to re-establish itself after interruption without the formation of a fracture callus".[20] However, secondary healing allows a more natural form of fracture healing to occur involving "hemorrhage inflammation, primary soft callus formation, callus mineralization, and callus remodeling".[20] This form of indirect bone healing results in bone formation that is more similar to the bone already present in the spine. An important outcome of secondary healing versus primary healing is that with the right amount of allowed motion the bone will heal in a matter of weeks compared to months or even years for primary healing.[21]

The final major difference between this design and current models in production today is that this final product will be made using 3D printed titanium (Ti-6Al-4V) from a third-party DMLS manufacturing machine. DMLS stands for Direct Metal Laser Sintering which involves a CO^2 laser sintering and fusing titanium powder to create a reliable metal part. This form of manufacturing creates accurate, small metallic parts with tolerances of approximately 20 – 50 microns.[26] This is of the utmost importance due to the porous nature of this design and the difficulty of constructing the complex geometry using traditional manufacturing processes. It is necessary that the complex geometry be formed as accurately as possible to achieve the expected material properties from the finite element analysis. This process has been used successfully to manufacture porous cages such as the Renovis Tesera Anterior Lumbar Interbody Fusion Cage (Renovis, Redlands, California) shown in Figure 10 below.

Figure 10: Lumbar fusion cage manufactured using DMLS.[17]

The Renovis cage was one of the first devices with a "true porous structure" and was manufactured using DMLS.[17]

II.vi Project Goals:

The lumbar cage that was designed will be able to support the same intervertebral forces as the disc it is replacing, similar to most cages already on the market. The three major differences between this design and most current models are that: 1) the design was modeled using patient-specific geometry; 2) it was effectively porous; and 3) it was manufactured using additive manufacturing. The goal of this project was to accomplish the three items stated above while remaining under budget and within defined structural criteria.

II.vii Design Criteria:

This design aims to optimize the porosity of a stand-alone lumbar cage while adhering to the following design criteria:

1. Have comparable graft volume to currently available all-in-one cages (~5000 mm^3)[17]
2. Support physiologic loads sufficiently, which is approximately 3000 N
3. Resist subsidence and migration
4. Have significant porosity to maximize surface area and achieve a modulus of 1.5 GPa

The objective is to optimize the material properties of this cage as shown in Table 1 below.

Table 1: Objective material properties for final design

Strain	Modulus [GPa]	Yield Stress [MPa]
2%	1.5	>600

III. METHODOLOGY

III.i Finite Element Analysis:

In order to accomplish secondary bone healing, the implant must be able to allow a minimum strain of 2% and a maximum of 10% as described by Perren's Strain Theory.[22] A strain of 2% will induce callus formation and begin the secondary healing process. To achieve a minimum strain of 2% the effective modulus of elasticity of the implant must be approximately 1.5 GPa for a 3000 N compressive load. The 3000 N load represents the compressive force of approximately four times the average male weight of 182 lb which is twice as large as the compressive forces felt by the lumbar spine while walking.[23][24] A 3000 N load was chosen to take into account daily forces that may increase that compressive load above the typical walking forces such as sitting, walking up stairs, or carrying a small amount of weight. Optimizing a patient-specific porous implant using finite element analysis is computer-intensive and time-consuming. In order to decrease the amount of time simulating full cage designs, a representative volume element (RVE) with a geometric volume of 1000 mm^3 is used to optimize the porosity

and effective material properties of the implant. To calculate the modulus of elasticity of this model the relationship between stress and strain was needed. The normal stress experienced by an object is defined as

$$\sigma = \frac{F}{A} \tag{1}$$

where σ is the stress experienced by the object in Pa, F is the applied force in N, and A is the area of the object perpendicular to the applied force in m^2. The strain of object due to that applied force is defined as

$$\epsilon = \frac{l - l_0}{l_0} = \frac{\delta}{l_0} \tag{2}$$

where ϵ is the engineering strain of the material, l_0 is the original length of the material, l is the final length of material, and δ is the deformation of the material. The relationship between the engineering stress and strain of the material is then further defined to be

$$E = \frac{\sigma}{\epsilon} \tag{3}$$

where E is the modulus of elasticity of the material. Therefore the final cage design must be porous enough to reduce the effective elastic modulus of the implant from that of titanium (118 GPa) to 1.5 GPa to achieve a 2% strain for a 3000N load over a 1 cm^2 area.[25]

The process of analyzing the effectiveness of each design iteration on the deformation and modulus of elasticity is through the use of static simulation and finite element analysis (SolidWorks, Lexington, MA). Once the material properties of the RVE reached the values in Table 1 through the use of a unique porosity, the effective properties were then applied to a solid cage to determine whether it would act like the model without requiring computer intensive

calculations and complex geometry. However this did little to help the design process and was not pursued. The untouched original RVE is shown below in Figure 11.

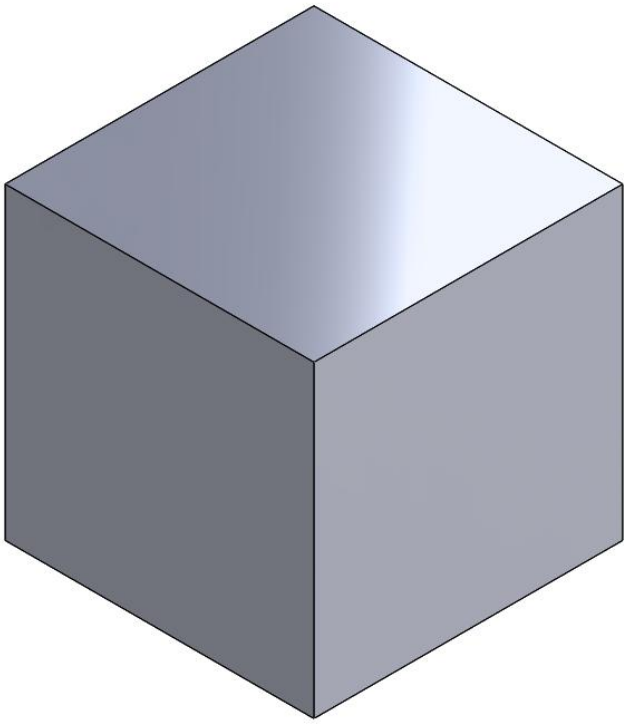

Figure 11: Original elemental model with volume of 1000 mm^3

This model acted as the baseline to all of the design iterations needed to optimize the effective material properties. It was representative of the pure titanium alloy and all of its associated properties. Each design progression maintained the same outer geometry as the model shown in Figure 11. At this point in the design, only compressive loading and normal strain was considered. In SolidWorks the loading was applied in the 'y'-direction, perpendicular to the top face. The RVE was then restrained with roller/slider fixtures on the two perpendicular faces in the 'x' and 'z' directions to allow for compression deformation while restricting any torsional

deformation that would not be experienced in a real life application. The baseline RVE in Figure 11 is shown with these forces applied in Figure 12 below.

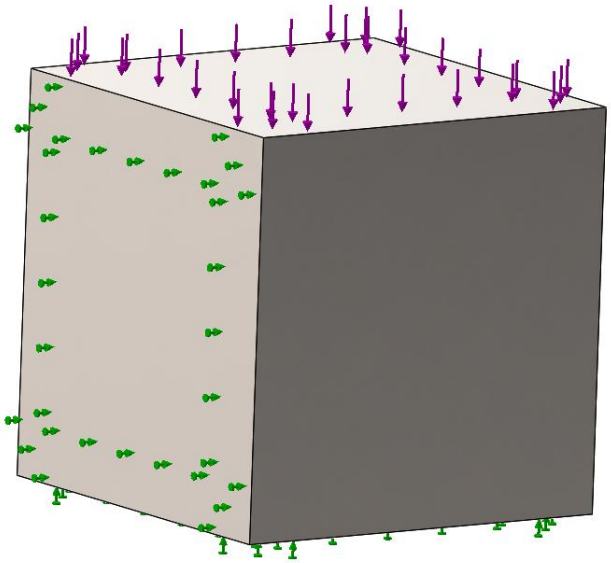

Figure 82: The forces applied (purple) and roller/slider restraints (green) on the baseline RVE

To calculate the strain due to the applied load, the average deformation of the top face was determined. Using (2), the strain was calculated by dividing the deformation by the original height of the RVE (1 cm).

The pore shape used for each design iteration was circular as opposed to square or triangular. It has been shown that circular pores reduce the stress concentrations present in rectangular or triangular pores while reducing the modulus just as effectively.[27] The first two iterations involved symmetrical pores cut through all three directions (x,y,z) of the RVE. The first iteration had 25, 1 mm pores on all three faces and the second had 81, 0.5 mm pores on all three faces. These are shown in Figure 13 below.

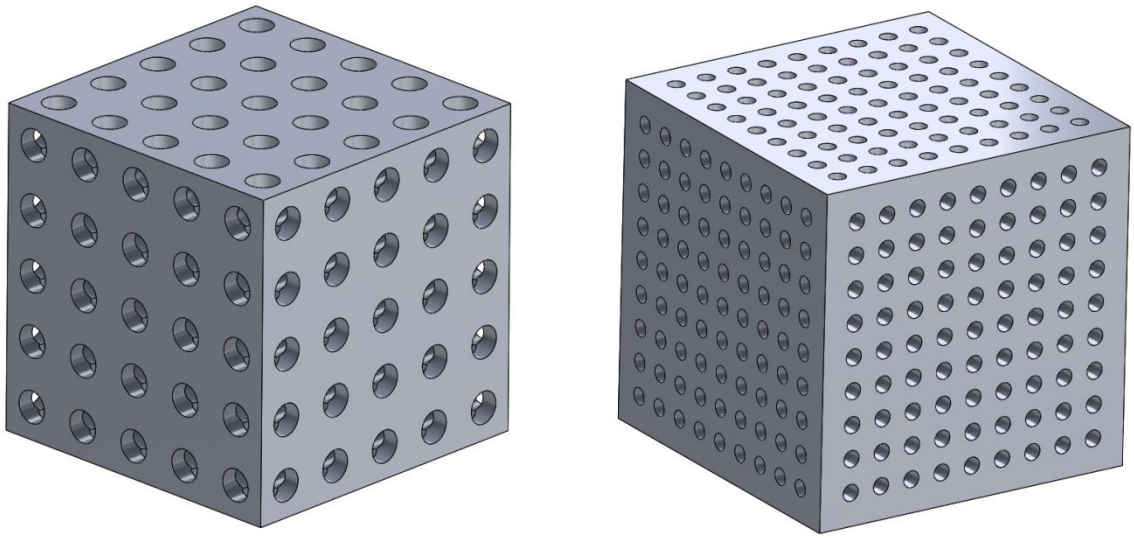

Figure 13: Initial design iterations with 1 mm pores (left) and 0.5 mm pores (right)

The 1 mm pores had a pore separation of 2 mm in each direction and the 0.5 mm pores had a pore separation of 1 mm from center to center. After applying the loads, the first step of the analysis was to create a mesh. Due to the porous nature of the RVE, the curvature based mesh was determined to apply the most accurate mesh possible while using it on the finest setting. An example of a curvature based mesh of the 0.5 mm porous RVE is shown in Figure 14 below.

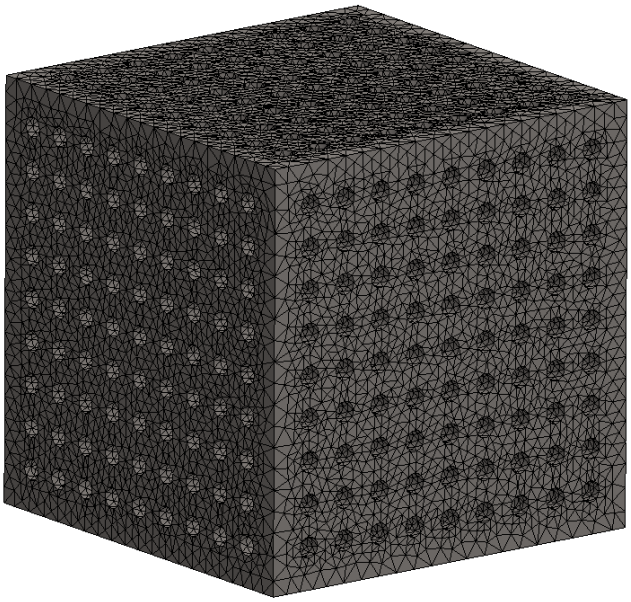

Figure 14: Curvature-based mesh of 0.5 mm porous RVE

As shown in Figure 14, SolidWorks automatically created more mesh elements in higher curvature areas such as is seen at the pore locations. Once an accurate mesh was completed the static analysis was run. Once an analysis had been completed, stress, strain, and displacement plots were automatically generated. Since this design is currently focusing on the deformation in the 'y'-direction, the deformation plot was adjusted to only represent the deformation in that direction. Using the "probe" tool on the top face of the RVE, the average deformation of the cube was determined.

Removing enough material in the right places decreases the modulus while maintaining structural strength.[27] Therefore the next design iteration was modeled off of a historically strong structure: the truss. The truss-like structure was chosen due to its successful use in the design of bridges and its ability to support large loads with minimum material. Four equal isosceles triangles were cut through the front face of the RVE to remove material and increase the allowed

strain. Then, utilizing the results from the 1 mm pores, the same 5x5 set of pores was added to the top and lateral faces of the design as shown below in Figure 15.

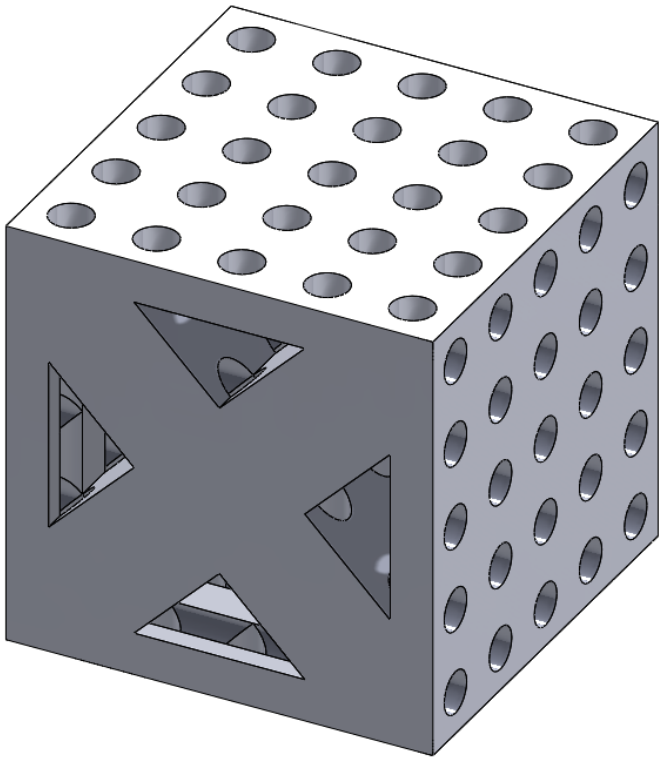

Figure 15: Truss style design with 'X' through front face.

The large triangular pores replaced the pores from Figure 13 through the front face and therefore had a similar porosity of 41.99%. However the new shape of the design had a significant effect on the modulus by decreasing it further to 23.72 GPa. Due to the positive impact that the ‘X’ design had on decreasing the modulus, Figure 15 became the new baseline RVE and further iterations maintained that general scheme of design.

III.ii Optimized Design Analysis:

The final design of the RVE involved a variety of sizes and separation distances of circular pores through each face while maintaining the central "truss" structure through the front face. The geometry of the top face was comprised of 36, 1 mm diameter circular pores in the formation shown in Figure 16 below.

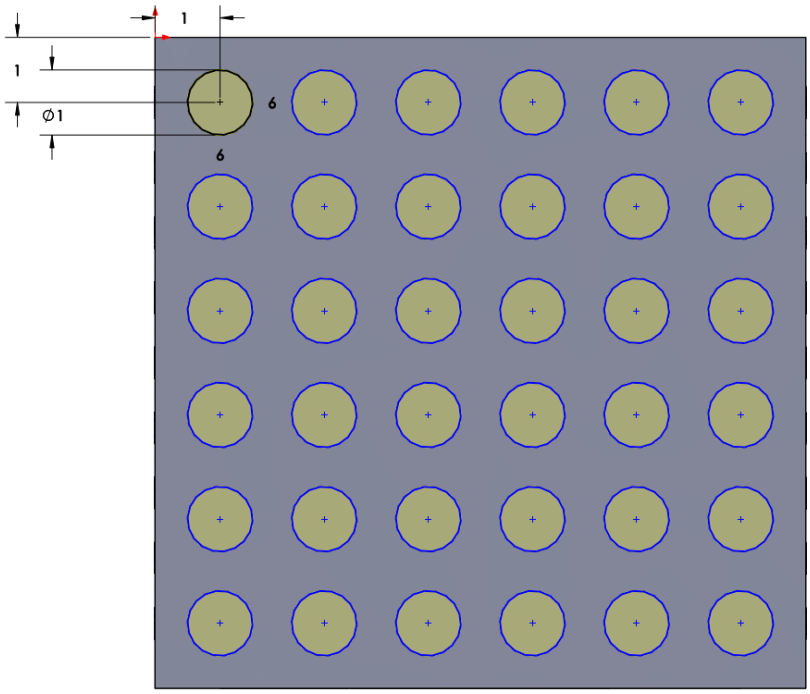

Figure 96: Geometry of top face of current design

These pores have a 1.6 mm separation between the centers of the pores. This allows for a 0.6 mm wall thickness which is satisfactory for the DLMS process.[26] The lateral face had similar geometry with 65, 0.5 mm diameter circular pores in a linear formation similar to Figure 15. In each corner of the linear formation there was a 2 mm diameter pore that is 1.5 mm from each side. This geometry is shown in Figure 17 below.

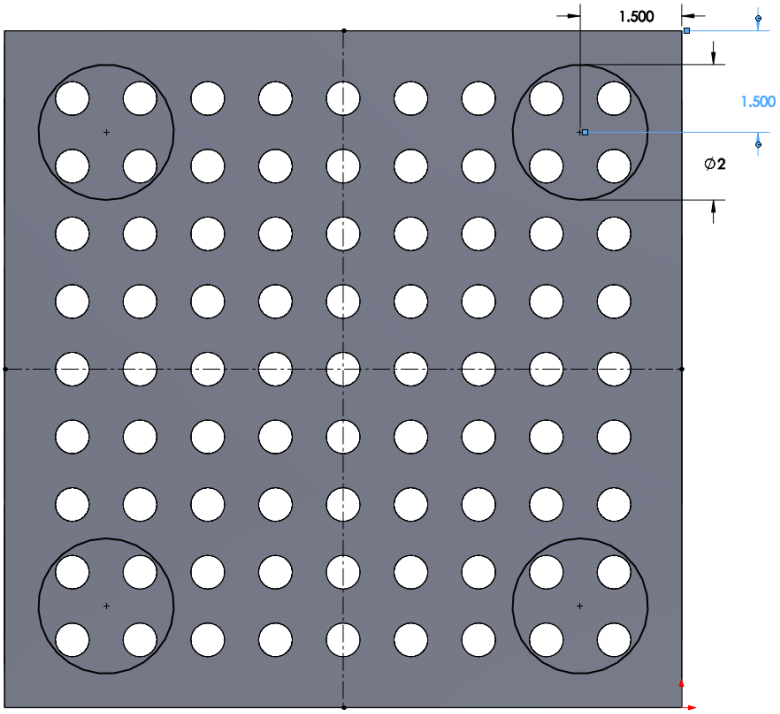

Figure 17: Geometry of the lateral face of the current design.

The front face had the most varied, and complex, geometry of the three faces and is shown below in Figure 18.

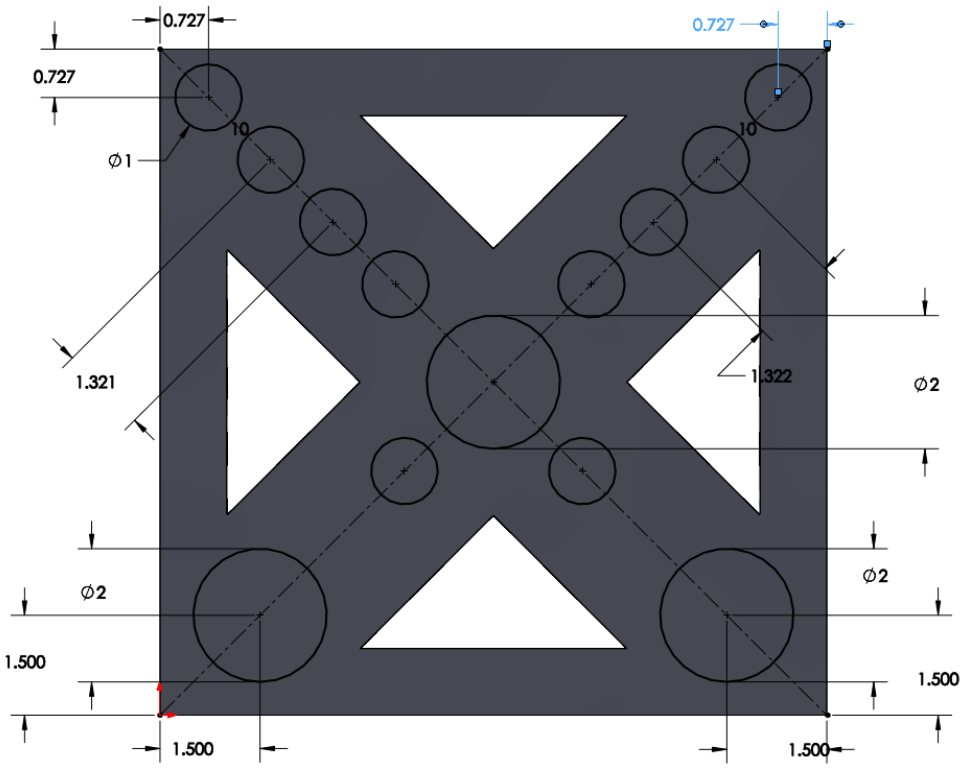

Figure 108: Geometry of the front face of the current design.

The front face consisted of five 1 mm pores centered on the diagonal axes of the with a 1.32 mm separation. The same triangles used in Figure 15 were still used in the final design to create the 'X' shape. Finally there were three 2 mm pores with one centered at the center of the RVE and the other two are 1.5 mm from each edge of the bottom two corners. The separation between the 1 mm pores was small enough to potentially result in a wall thickness too thin for the DMLS process causing an incomplete thickness being formed.[27] An isometric view of the final design is shown in Figure 19 below.

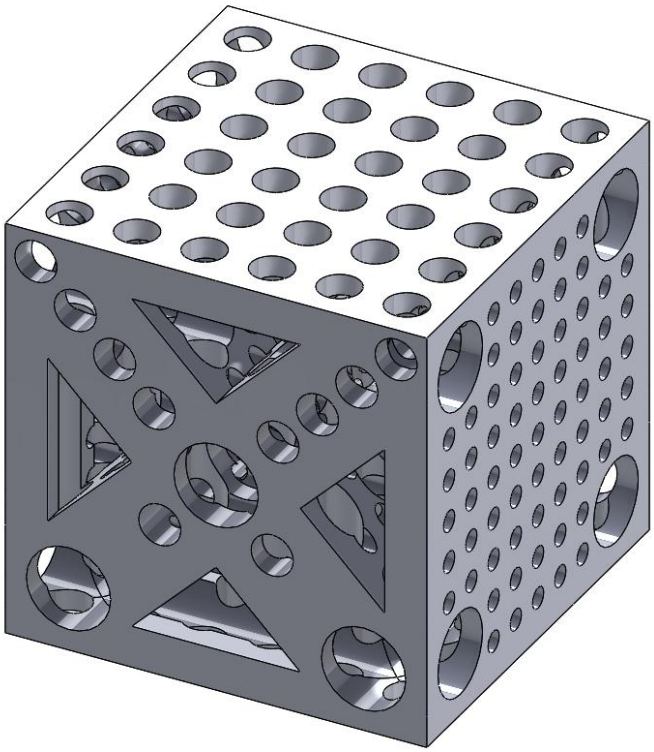

Figure 19: Isometric view of current RVE design.

IV. PRELIMINARY RESULTS

IV.i Preliminary Design Iterations:

When the static analysis was run on the mesh shown in Figure 14 it resulted in the deformation plot shown below in Figure 20.

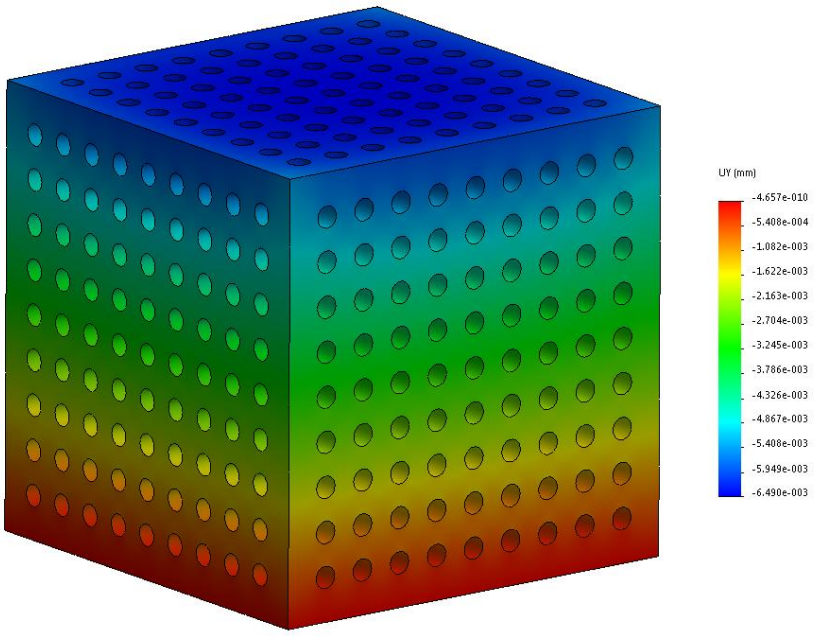

Figure 20: Deformation plot in the 'y'-direction with deformation scale

The average deformation on the top face was determined to be -.0075 mm which corresponded with a -0.075% strain, a porosity of 41.23%, and a 39.97 GPa modulus. This result is already a large improvement on the modulus of the baseline RVE which had a deformation of -.0029 mm and a modulus of 104.8 GPa.

IV.ii Optimized Design Analysis:

The design iterations based on Figure 15 are shown in Figures 21-24 below in the order in which they occurred.

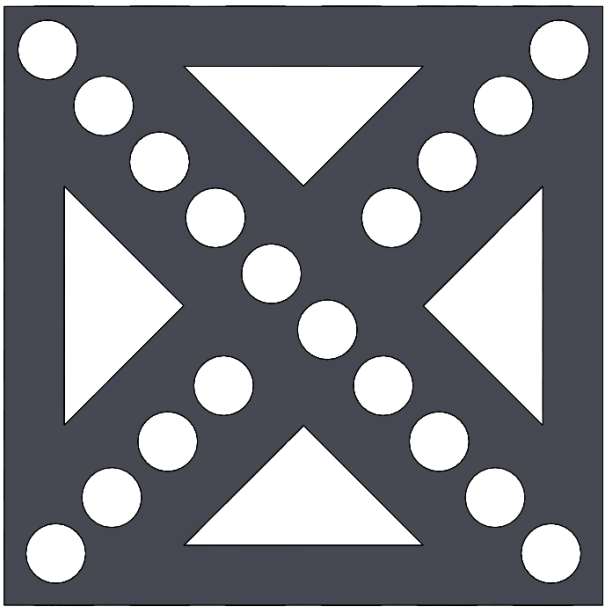

Figure 21: Same design as Figure 15 but with 1mm pores through "X" with 1.3mm separations

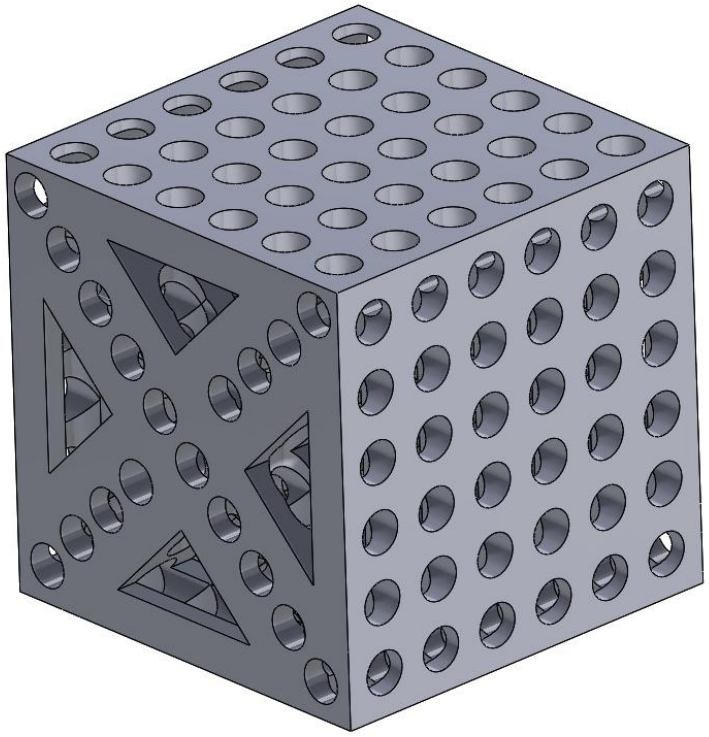

Figure 22: Same design as Figure 21 but with 6x6 1mm pores with 1.6mm spacing.

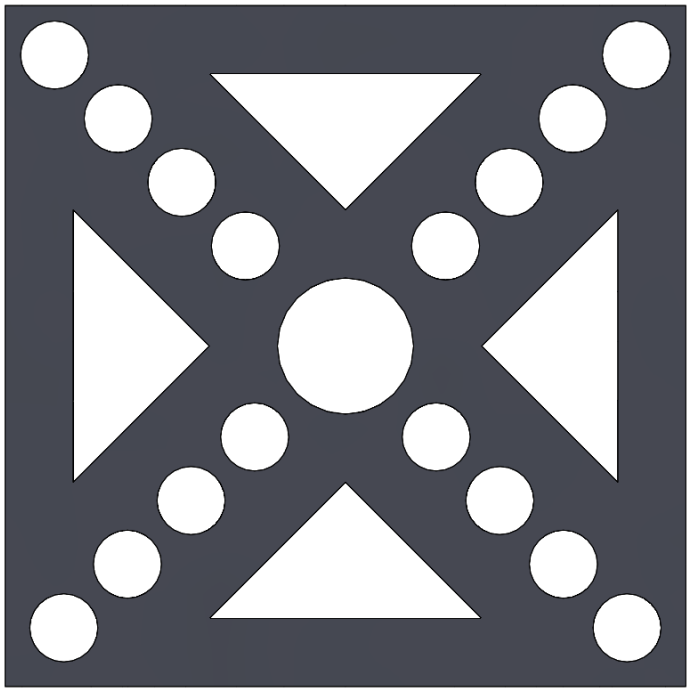

Figure 23: Same design as Figure 22 but with 2 mm pore through center of 'X'.

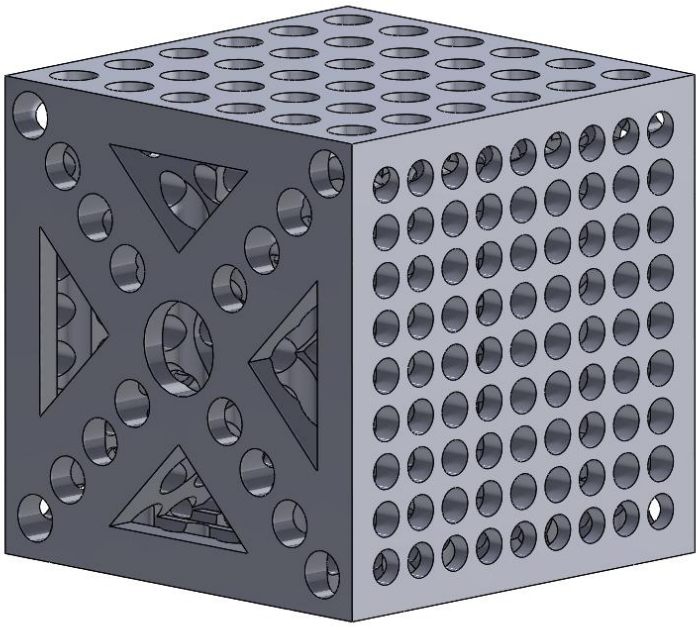

Figure 114: Same design as Figure 23 but with 9x9, 0.75mm lateral pores.

Table 2 displays the deformation, strain, modulus, and porosity of the design progression.

Table 2: Material properties of each design iteration with a 3000 N applied compressive load

Design Iteration	Stress (MPa)	Deformation (mm)	Strain (%)	Modulus (GPa)	Porosity (%)
0	30	0.0029	0.03	104.7998	0
1	30	0.0075	0.08	39.9712	41.2300
2	30	0.0126	0.13	23.7229	41.9860
3	30	0.0189	0.19	15.9033	51.9860
4	30	0.0224	0.22	13.3654	59.2034
5	30	0.0231	0.23	13.0112	60.1860
6	30	0.0379	0.38	7.9053	66.8810
7	30	0.0425	0.43	7.0528	62.1590

The final design yielded a strain of 0.43% and a modulus of 7.1 GPa with a porosity of 62.2%. This modulus is much closer to the goal of 1.5 GPa and a strain of 2% than what the RVE started with. Throughout the design progression it was determined that there exists a linear relationship between the modulus and the porosity as shown below in Figure 25.

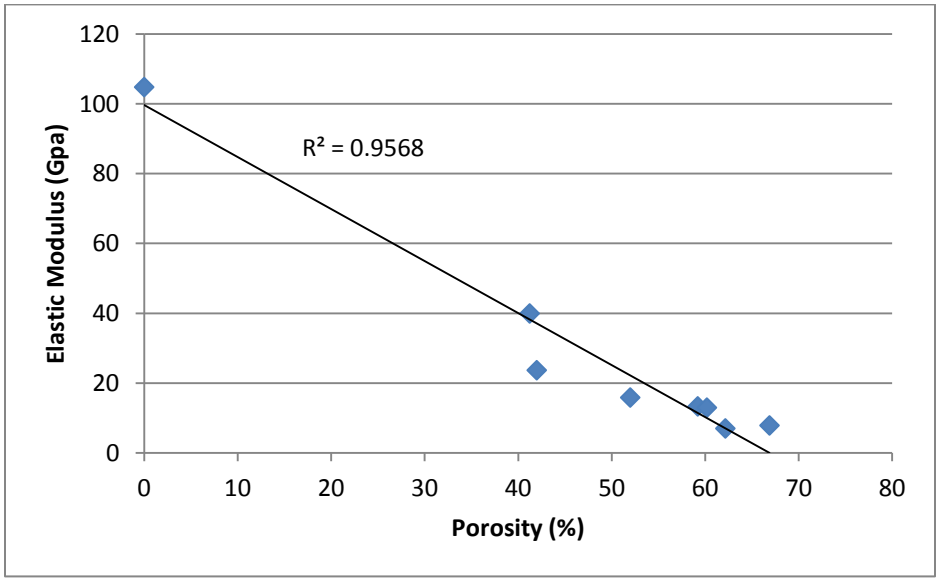

Figure 25: Relationship between porosity of the RVE and its elastic modulus

As shown above the porosity of the RVE had a significant impact on reducing the modulus. The relationship is nearly completely linear with a goodness of fit (R^2 value) of 0.9568 which shows there is little variance beyond the linear relationship.

V. DEVELOPMENT OF THE PATIENT SPECIFIC CAGE GEOMETRY

V.i Image Segmentation:

A CT scan of a person's lower spine from T12 to S1 was provided to be converted into a SolidWorks model. The CT scan data was exported as many thin slices as dicom files. The slices contained the data for the patient's bone, soft tissue, blood vessels, muscle, etc. and it was necessary to only include the lumbar bone data when exporting. In order to do this, a program was used to adjust the files to only view the L4 and L5 vertebral bodies and then exported that data into a file type that SolidWorks could read. First, the free open-source program 3D Slicer was evaluated to determine if it was a suitable program for this project. Although it had a variety of useful tools and features, it was determined to not be a suitable match for these purposes due to its inability to reduce the size of the mesh. When importing an .stl file into SolidWorks as a solid body the file size must be kept small. Due to the complexity of the three dimensional mesh created by 3D Slicer the files were too large to import into SolidWorks. However 3D Slicer is an effective program for the use of models used for visualization as opposed to design work.

A trial license was attained for the medical image processing software, Mimics, and its partner design software, 3Matic (Materialise, Leuven, Belgium). Using Mimics, the CT scan data was imported and was visualized in the program in the sagittal, coronal, and transverse planes. The Mimics interface with the data shown in the three body planes is shown below in Figure 26.

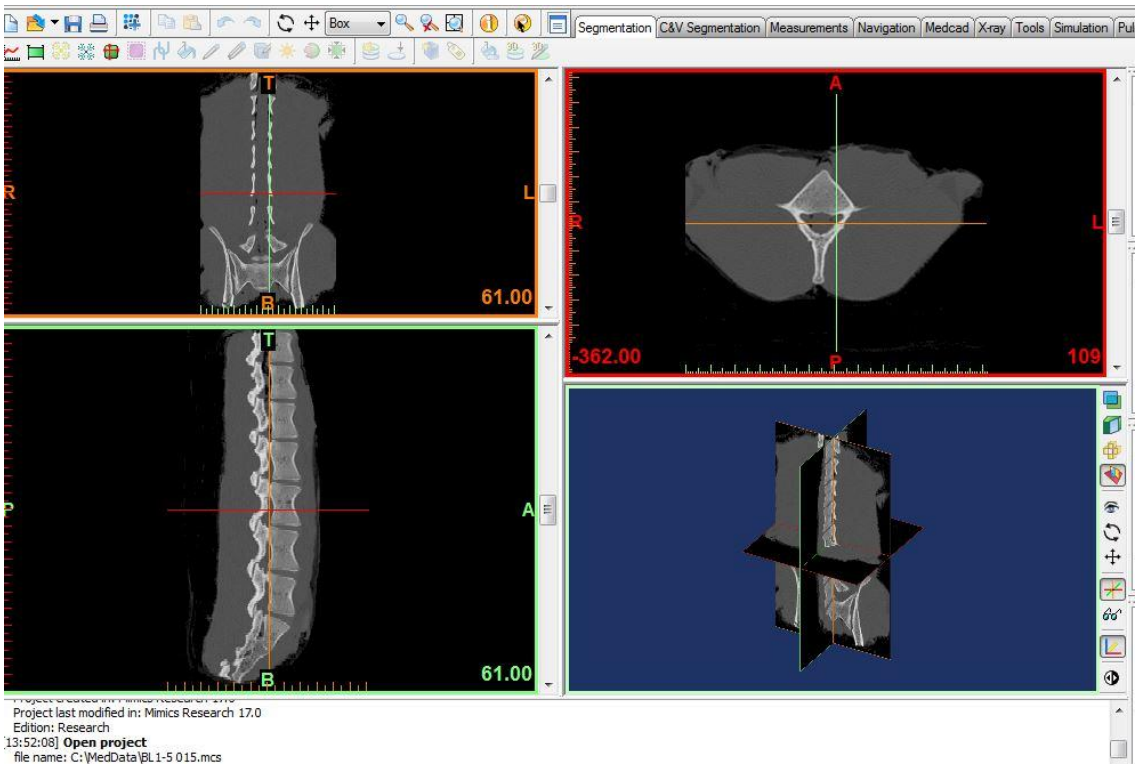

Figure 26: Mimics CT data shown in the coronal (Upper Left), sagittal (Lower Left), and transverse (Upper Right) body planes.

When the CT data is initially imported into the program it contains all of the information about the patient including bone, soft tissue, and muscle. When a CT scan is performed, different parts of the body absorb different amounts of radiation. The amount of radiation that different objects can absorb is measured in terms of Hounsfield Units. Compact bone is well known to absorb a large amount of the energy emitted.[28] Mimics had a feature that allowed the user to threshold the parts of the CT scan shown based on a range of Hounsfield units. Using the predefined bone threshold preset by Mimics, a threshold range of 226 to 2275 Hounsfield units was used to separate the bone from the rest of the components of the body. Mimics completed this by creating a green "mask" on the three body planes. Once this was done, the "crop" function was used to select one of the vertebral bodies of interest (either the L4 or L5). The Mimics interface showing the CT data post-thresholding is shown below in Figure 27.

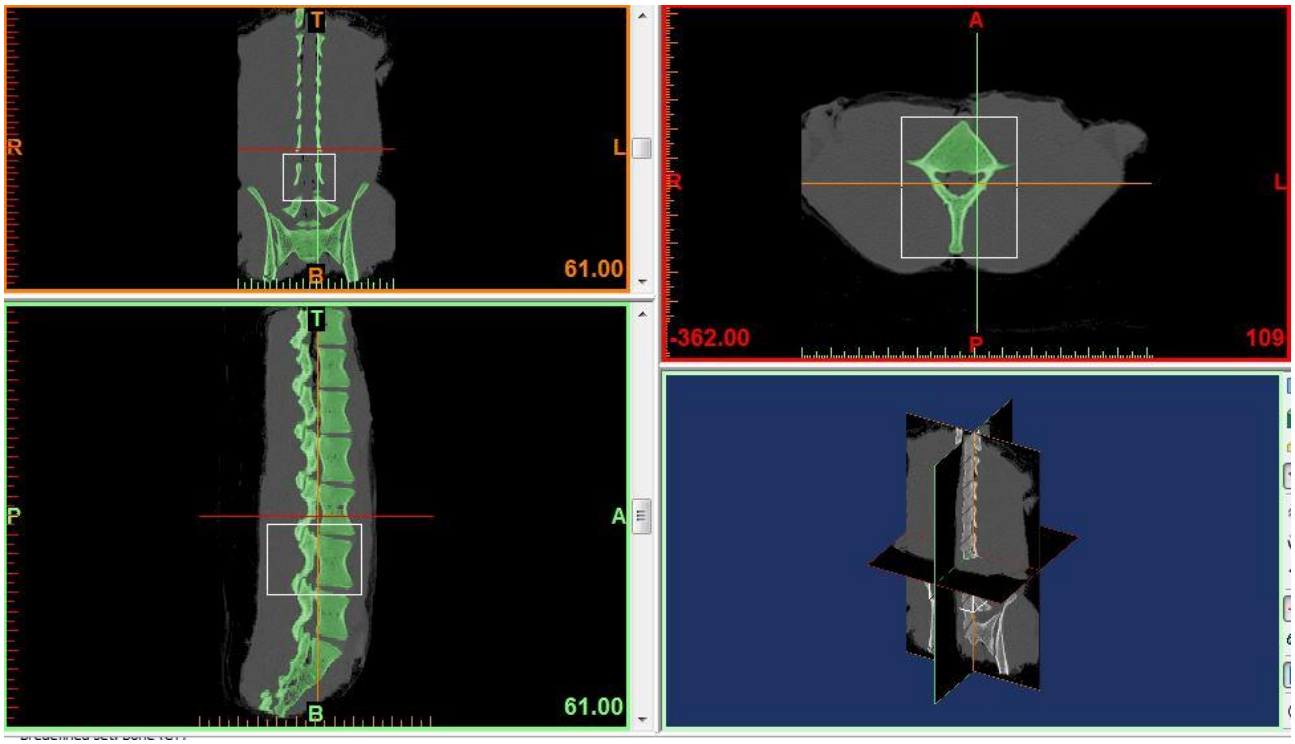

Figure 27: CT scan data highlighting the compact bone in green.

The white box shown above in each of the body planes is used to crop the mask to the necessary size. Due to limitations on the crop by the geometry of the crop tool, there were portions of neighboring vertebral bodies included in the new cropped mask. Using the feature "multiple slice edit" it was possible to edit out unwanted sections from the mask by interpolating over multiple two dimensional slices. Once this was completed the feature "region growing" was used to clean up the mask. Region growing requires the selection of one pixel within the desired mask which then connects to all neighboring pixels to create a more accurate mask. This entire process was completed for both the L4 and L5 vertebral bodies. The completed mask of the bodies with the adjacent 3D model is shown below in Figure 28.

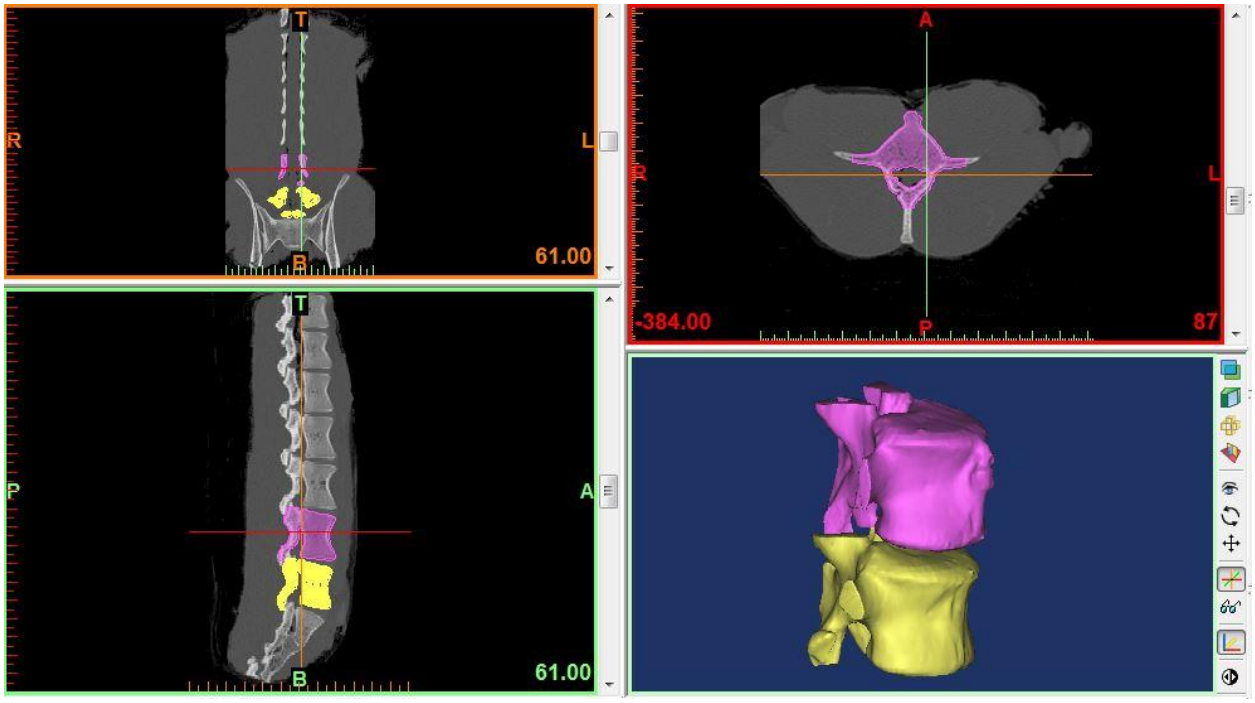

Figure 128: The completed masks of the L4 and L5 vertebral bodies with the associated 3D model.

V.ii Model Orientation:

Once the 3D model was generated it was exported into 3Matic in order to alter the orientation of the bodies between each other. The average distance between the endplates of the vertebrae on the anterior side, also known as the disc height, was approximately 6.5 mm. The average disc height for an adult is approximately 11.3 +/- 2.1 mm, suggesting that this patient was suffering from disc degeneration. When performing a spinal fusion procedure in the lumbar it is necessary for the surgeon to reestablish a healthy disc height at the pain location. Another issue with the orientation of the bodies was that the endplates were nearly parallel to one another. Current cages are designed to restore a healthy angle of lordosis to the bodies in question. The angle of lordosis of current cages often range from five to twelve degrees.[30][31] Based on cages currently in use today, a cage with a twelve degree lordotic angle was chosen. When the Mimics file was imported into 3Matic the model was rotated to adjust the angle between the two

endplates to 12 degrees, and then translated to have a disc height of approximately 12 mm. Figure 29 below shows the final orientation of the L4 and L5 vertebral bodies.

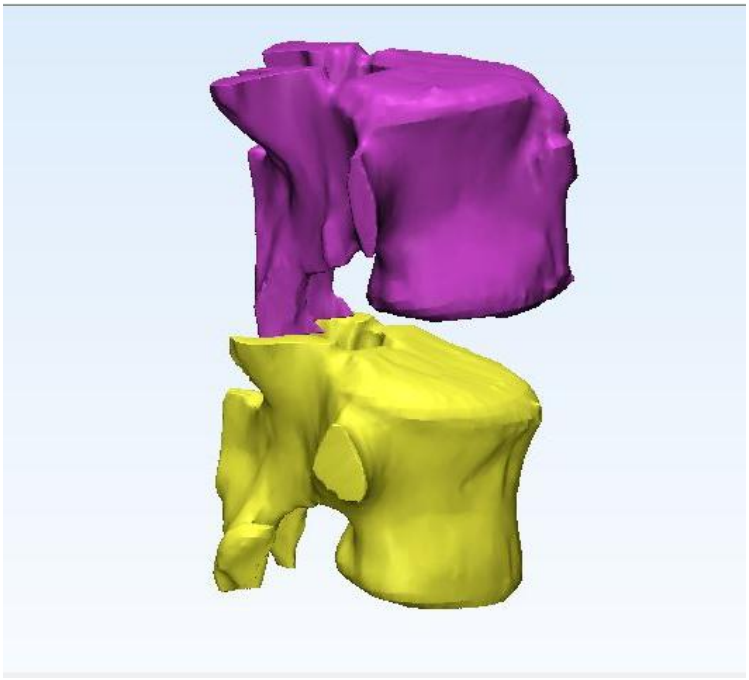

Figure 139: Final orientation of the L4-L5 vertebral bodies.

The greatest impact that Mimics/3Matic had on the image segmentation of the vertebral bodies was the ability to simplify the 3D mesh. Using the "Auto Rectangular Patch" feature on 3Matic, the typical triangular mesh making up the bodies was replaced by a rectangular patch mesh. The new mesh maintained the integrity of the 3D model while reducing the actual size of the file. Once this was all completed, the 3matic file was exported as a .iges file to be imported into SolidWorks. The vertebral bodies imported as a part file in SolidWorks are shown in Figure 30 below.

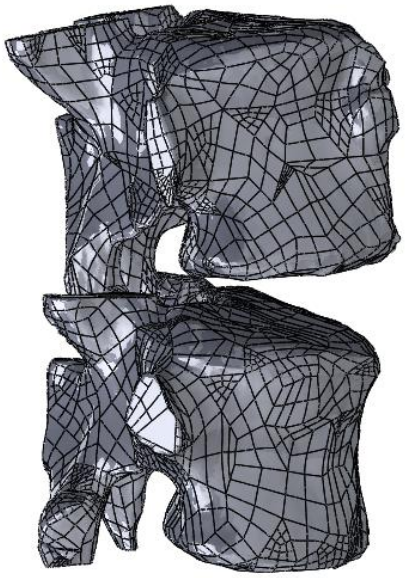

Figure 30: SolidWorks model of the L4-L5 vertebral bodies.

VI. FINAL DETAILED DESIGN

VI.i Detailed Design:

The final cage design consists of two separate parts held together by four pegs on the top piece coinciding with four holes on the bottom. This choice was made to allow the superior aspect of the cage to be removed and the central region of the cage to be filled with graft material. The graft space would then be contained within the cage itself without losing as much endplate contact surface area as other cages do. Each part has the same outer 30 x 20 mm rectangular geometry, designed to fit the specific patient geometry well. The two parts were extruded to their associated endplate from two separate planes that were six degrees from each endplate. Extruding up to each endplate created the patient specific geometry of the top and

bottom faces of the cage while keeping the cage mostly symmetrical. The solid cage is shown below in Figure 31.

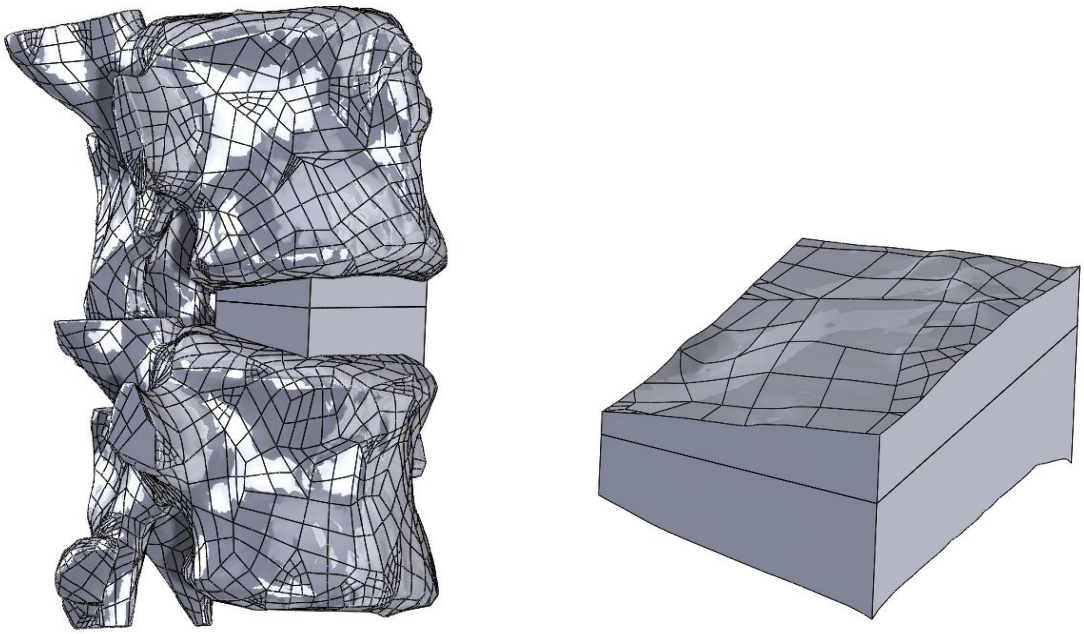

Figure 141: Solid cage geometry in the assembly (Left) and out (Right) with patient-specific endplates with the anterior side facing right.

The first modification to the cage was creating the truss structure shown in the RVE in Figures 15-24. The anterior (front) face of the cage is 30 mm long and approximately 14 mm high. Since the RVE geometry was a 10 x 10 x 10 mm cube, the truss geometry was able to be replicated three times across the anterior face. Initially, the same triangular geometry used in the RVE was used however later in the design testing the triangles were made larger to increase the amount of material removed. The truss width is 1.5 mm with a 2 mm separation between each set of trusses. Three truss sections made from four equal isosceles triangles each were cut into the cage 10 mm deep and are shown in Figure 32 below.

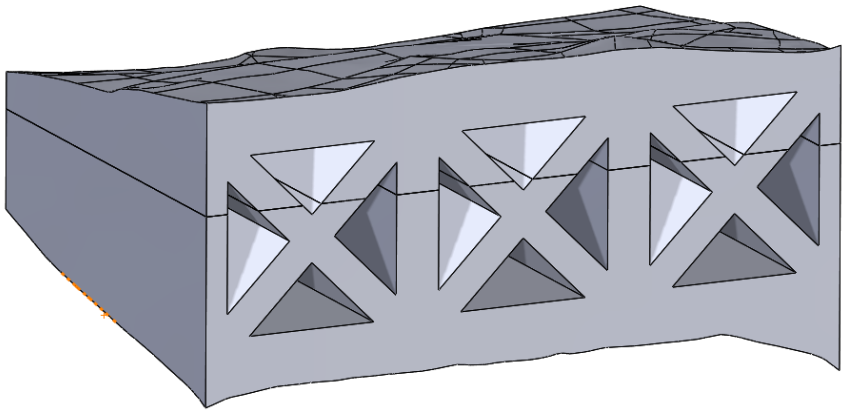

Figure 32: Cage with new truss structure through the anterior face.

An important feature of a fusion cage is the graft space. While most cages used today have large open graft spaces (see Figure 7), this cage's design keeps the graft space enclosed within the cage so as to maximize the contact area between the cage and the endplates. In the final design there are pores parallel to the endplates allowing bone growth to occur even without the open graft space. A graft space was created using two equal slots and extrude cut at angles parallel to the overall cage angle. This allowed for the maximum graft space possible while maintaining an approximately constant thickness on the top and bottom faces of the cage. The total graft space volume created by the slots is 1600 mm^3. Although this value is lower than the desired graft space of 5000 mm^3, the size of this cage is smaller than the average cage size due to this patient's lumbar geometry. Also due to other pore structures used the graft space could potentially be larger and will be discussed further in this section. A section view of the transverse plane showing the cage graft space is shown below in Figure 33.

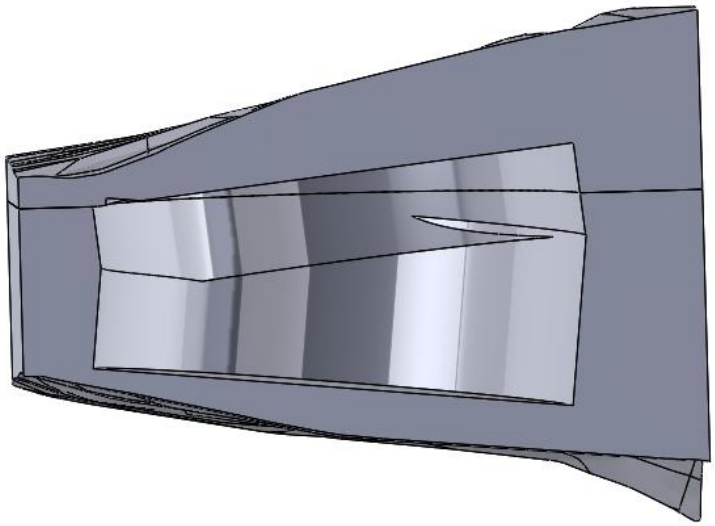

Figure 33: Section view of the cage, displaying the graft space graft space.

The next set of pores added to the cage were through the anterior and posterior faces and taken directly from the RVE geometry. The pores through the posterior were 1 mm diameter with a pore separation of 1.5 mm. Due to the decrease in the truss thickness the pores used in the RVE in Figure 23 were reduced in size and spacing. The diagonal pores through the trusses have a 0.5 mm diameter with a 1 mm pore separation. There is also a 1.25 mm pore through the center of each set of trusses. These pores can be seen below in Figure 34.

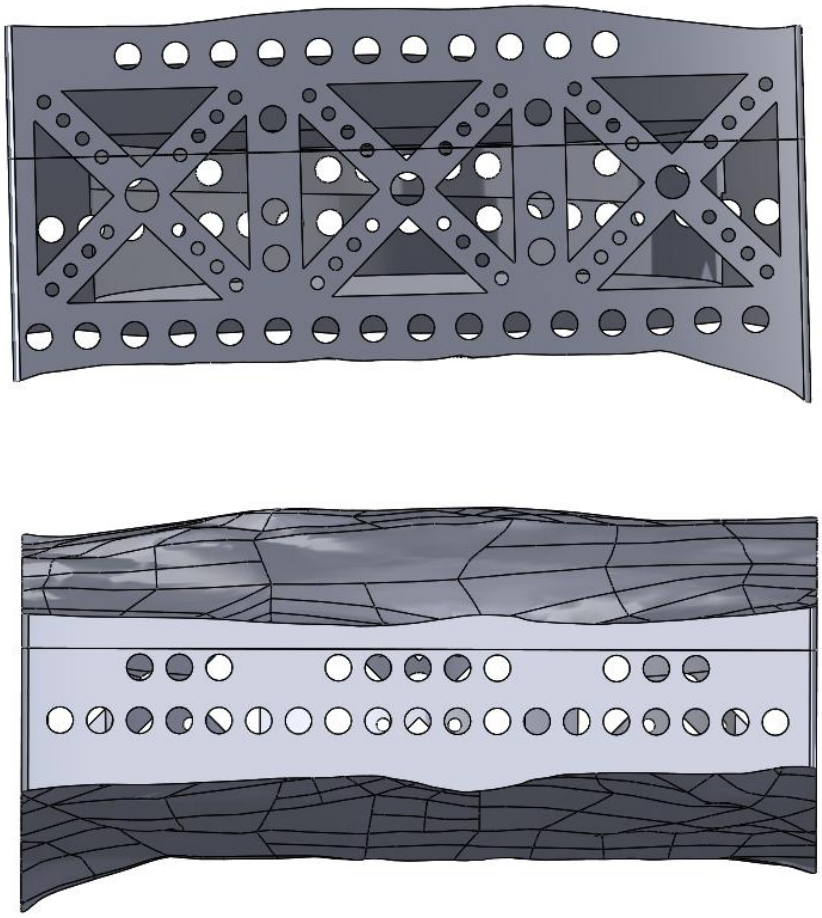

Figure 154: Anterior (Top) and posterior (Bottom) pores.

Due to the pegs holding the two parts together there are gaps in the pore structure on both the anterior and posterior faces to prevent the pores from cutting through the pegs. Next, 1 mm pores with a separation of 1.5 mm were cut into the lateral faces of the cage. One of the greatest improvements to the cage design from the RVE was the inclusion of a large opening on both sides of the cage. Including the slot-shaped opening removed much more material, greatly reducing the effective modulus of the cage. The oval slot is 3.93 mm tall by 16.75 mm wide and the slot and the pores extrude cut through the entire body. The only exception is four of the pores

that would otherwise intersect with the pegs attached to the top part of the cage. A side view of these pores is shown below in Figure 35 below.

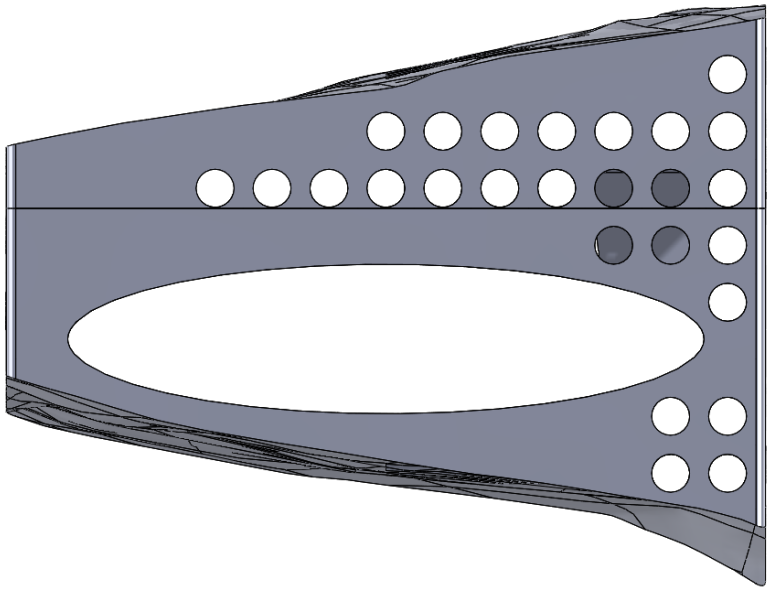

Figure 35: View of the circular and elliptical pores cut through the cage.

The final pores added to the design run through the top and bottom faces of the cage. These pores are crucial for fostering bone growth between the bone graft and the adjacent vertebral body endplates. The pore geometry of these faces is also important because it will be carrying most of the physiologic load applied. The majority of the pores going in this direction are the same geometry as the top face of the RVE shown in Figure 25 except the pore spacing is 1.5 mm as opposed to 1.6 mm. There are also 6, 4 mm pores in the center of the of the top face with a pore separation of 5 mm. The top view of the cage and an isometric view of the full cage design are shown below in Figures 36 and 37 respectively. An isometric view of each part separately with important features noted are shown below in Figures 38 and 39.

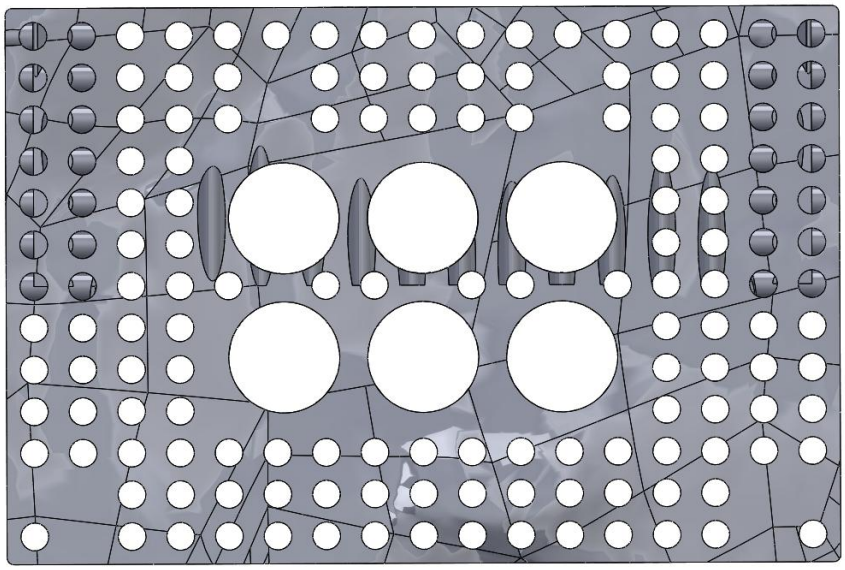

Figure 166: Top face of the fusion cage, top edge is the anterior

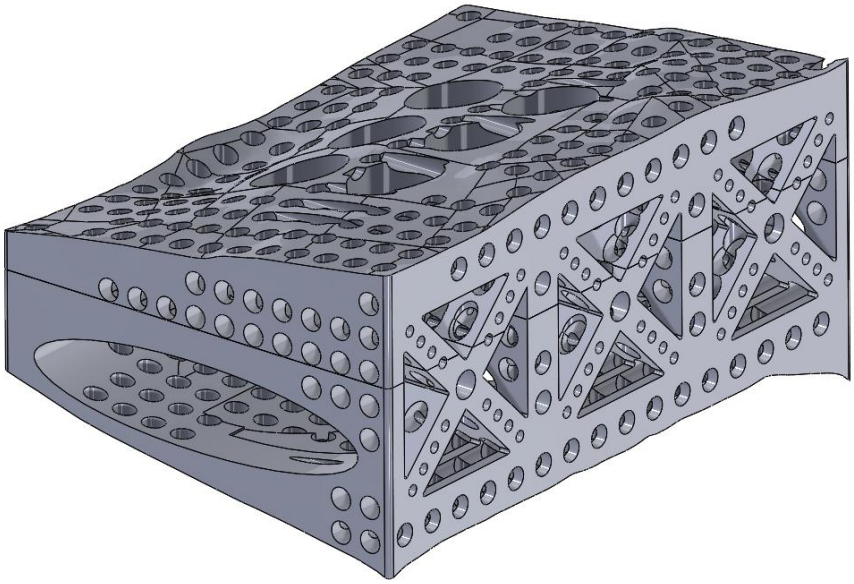

Figure 37: Isometric view of final design of fusion cage.

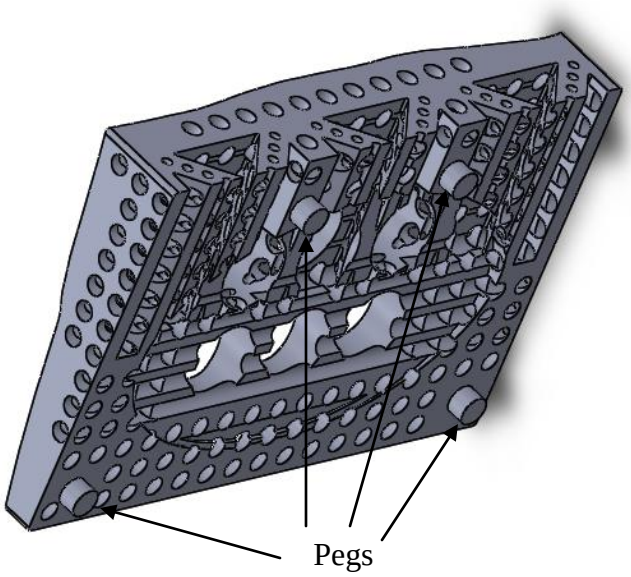

Figure 38: Top part of cage displaying the pegs used to connect the two parts.

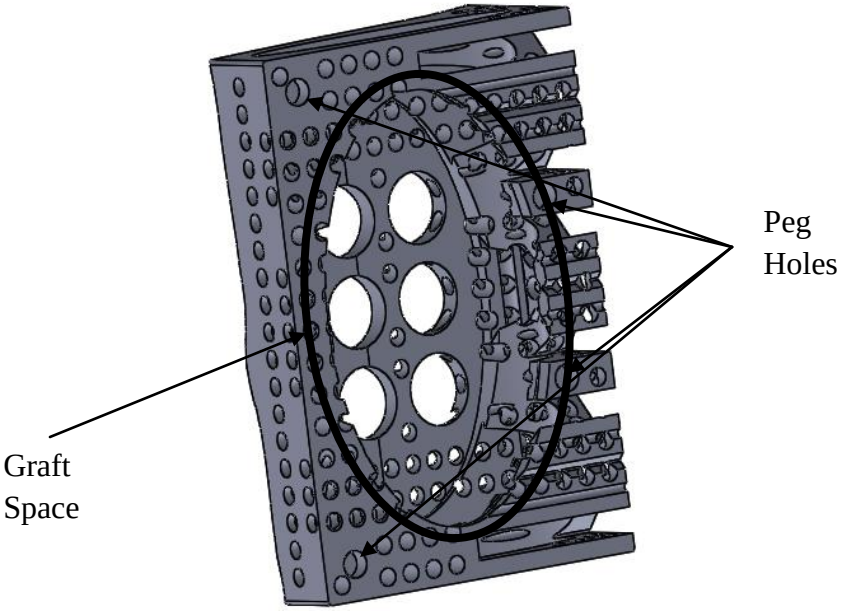

Figure 39: Bottom part of cage displaying the four holes to support the pegs of the top part.

VI.ii Final Design Analysis:

The cage iterations were analyzed using the same Finite Element Analysis (FEA) as shown in Figure 12. A roller-slider fixation was used on the left face of the cage to prevent any twisting that would not naturally occur. Although during preliminary FEA analysis of the RVE a

roller-slider fixation was also used on the bottom face, due to the complex geometry of the bottom face it was only possible to simply fix the entire side. It was determined that this did not have any major impact on the accuracy of the analysis. When screws are eventually used to fixate the cage it would be sufficiently rigidly fixed on to the bottom endplate. The same 3000 N physiologic load used for the RVE was applied to the top face of the cage. However due to the complex geometry a vertical load was applied. After the forces and fixations were applied, a curvature based mesh was performed on the finest setting to get the most accurate results with an element size of 0.573±0.03 mm, 553226 total nodes, and 331032 total elements. The curvature based mesh was used as opposed to the default mesh because it creates more mesh elements at circular and cylindrical faces. The completed mesh with fixations and forces shown is shown in Figure 40 below.

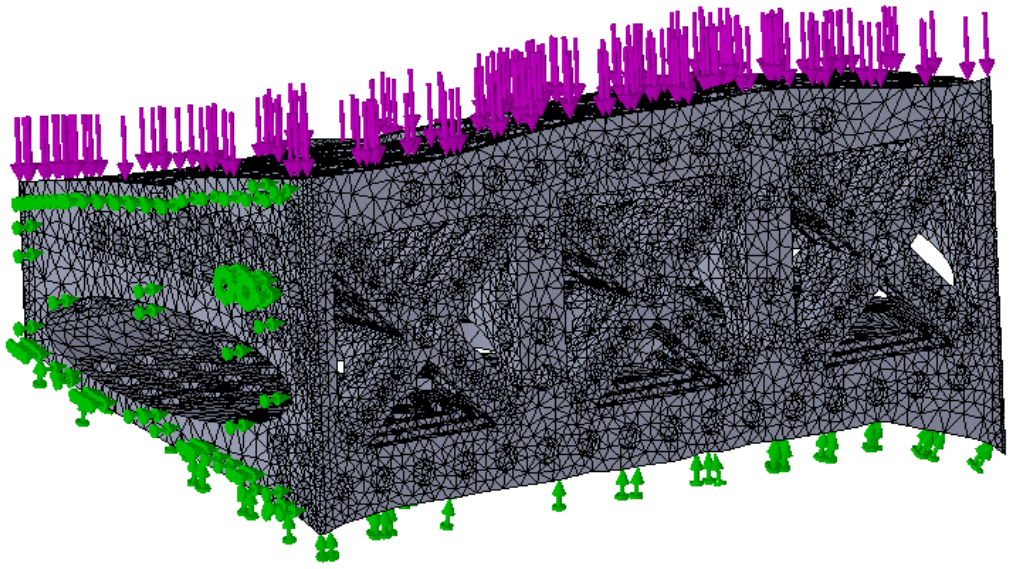

Figure 40: Cage after curvature based mesh with forces and fixations shown.

Once a mesh was completed, the FEA analysis was completed to simulate the loading under the required conditions. In this analysis only the deformation parallel to the applied force was of interest. Since the bone graft is stored within the center of the cage in direct contact with the top face, the average deformation of the top face was calculated to determine the effective elastic modulus of the cage. The average height of the cage was 10 mm and therefore the average deformation divided by the average height resulted in the average compressive strain in the direction of the applied force. The average deformation of the top of the cage was determined through the use of the probe tool on SolidWorks. When a face is selected the probe would display the average deformation in the direction chosen. To determine the average of the entire top of the cage each face was selected using a single probe tool to average the deformation. Then using Equation 3 the effective modulus of the cage was determined.

VI.iii Final Design Results:

The deformation, strain, and modulus were calculated for the center of the top face of the cage and the cage as a whole. It is important to know the average modulus and deformation of the center of the cage because it is directly above the graft space. Plots of the deformation of the cage in the direction of the force and the average von Mises stresses are shown in Figures 41 and 42 below respectively.

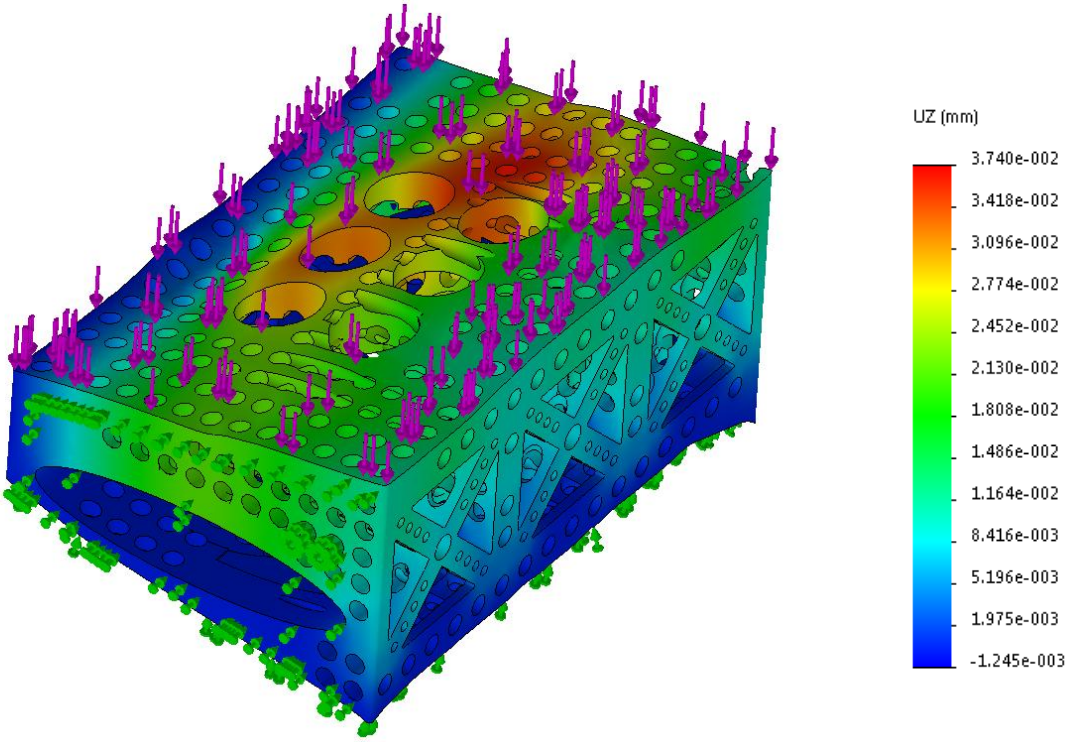

Figure 41: Deformation plot in the direction of the applied force.

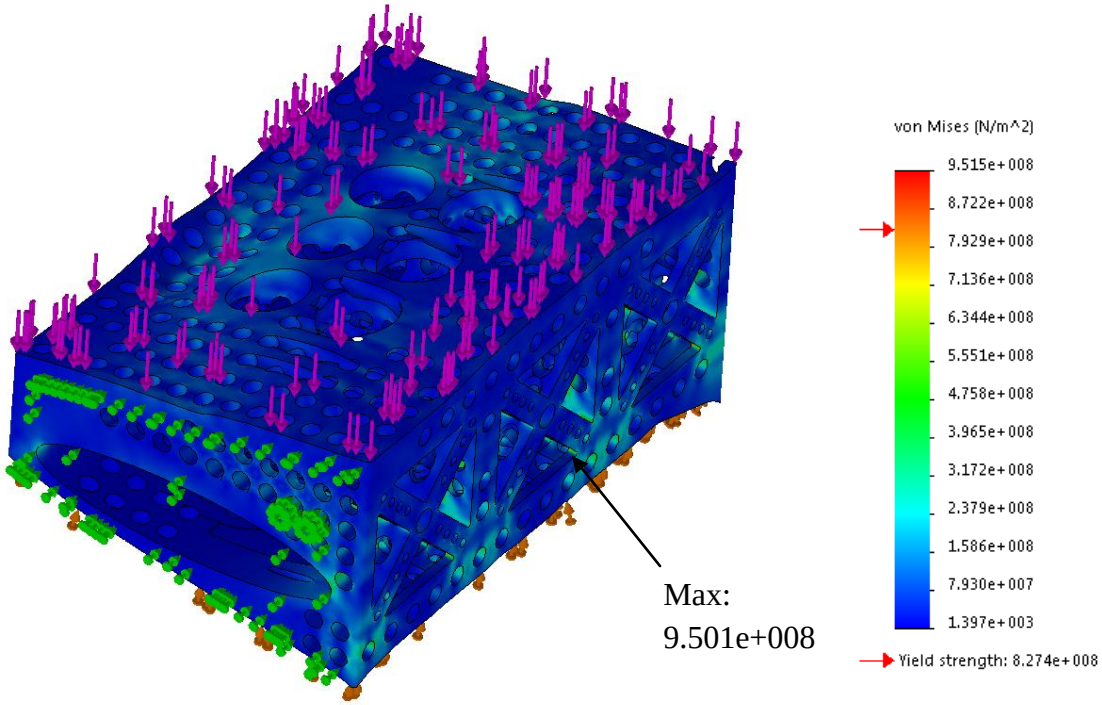

Figure 42: von Mises stress plot of the entire cage with maximum stress location noted.

The 3000 N force was applied over the rectangular area of the cage equal to 600 mm^2. Using Equation 1 the applied stress was determined to be 5 MPa. The average deformation and strain of the center of cage was 0.030 mm and 0.3% respectively. Using Equation 3 the effective modulus of the center of the cage was 1.67 GPa. The average deformation and strain of the entire cage was 0.019 mm and 0.19% respectively. The effective modulus of the cage was determined to be 2.58 GPa with an overall cage porosity of 69.9%. Table 3 below summarizes the final results.

Table 3: Final results for the FEA analysis of the fusion cage.

	Stress (MPa)	Deformation (mm)	Strain (%)	Modulus (GPa)	Porosity (%)
Center of Top Endplate	5	0.030	0.300	1.669	69.939
Total Top Endplate	5	0.019	0.200	2.576	69.939

The final elastic modulus of 2.576 GPa has a percent difference of 52.8% to the design criteria value of 1.5 GPa shown in Table 1 but is an improvement on the modulus of untouched titanium of 114 GPa.[27] The strain is lower than the desired strain of 2% to foster secondary healing, however it is progress and shows potential for further research. The cage mostly experienced stresses less than the endurance limit of 600 MPa with the exception of a few stress concentrations. Experimental testing will determine if the areas of high stress will or will not be problematic.

The porosity of the design played the largest role in reducing the effective modulus and increasing the strain of the cage. The different pore structures, shapes, and locations all played a vital part in the final effective cage properties. Since the relationship between strain and elastic modulus is linear, it was hypothesized that the relationship between the cage porosity and strain

(and therefore modulus) would also be linear. An FEA analysis was performed on the cage each time a new pore structure was introduced and that data is shown in Table 4 below.

Porosity Variation	Stress (MPa)	Deformation (mm)	Strain (%)	Modulus (GPa)	Porosity (%)
0	5	0.004	0.000	115.650	0
1	5	0.006	0.000	79.443	7.308
2	5	0.011	0.000	46.011	17.539
3	5	0.039	0.000	12.890	29.558
4	5	0.042	0.000	12.045	32.469
5	5	0.055	0.001	9.139	37.373
6	5	0.072	0.001	6.928	54.095
7	5	0.175	0.002	2.860	67.981
8	5	0.194	0.002	2.576	69.939

However the experimental results showed a near asymptotic relationship between overall porosity and elastic modulus. A plot of the relationship between the porosity and the modulus of the cage is shown below in Figure 43.

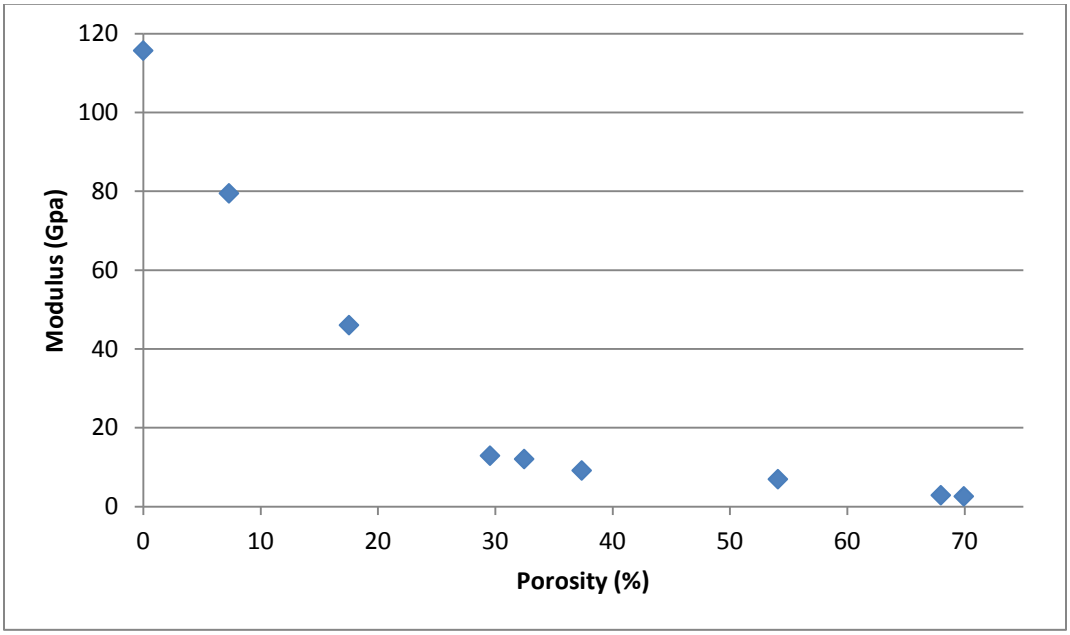

Figure 43: Plot of the relationship between porosity and elastic modulus of the cage.

The second and third data points of the plot from the left represent the initial and final truss sizes of the cage. These structures did the most to decrease the modulus without a large increase in porosity. If these points were eliminated from the plot the trendline of the remainder of the data points would have an R^2 value of 0.975 which is a good fit for the line. This plot demonstrates that the shape and location of the pore affect the overall modulus of the cage in different ways.

VI.iv Discussion of Final Results:

The ability to design a cage with patient-specific endplates through the use of biomedical imaging and 3D design software was confirmed as a feasible means of lumbar fusion cage design. With patient specific faces the amount of time a patient is in surgery is decreased which in turn decreases the chance of infection as well as the amount of time needed to recover. It is also effective at distributing physiologic loads and reducing stress concentrations. Having the graft space contained within the cage itself is unique and allows for an increased contact area between the cage and the endplate. However the graft space volume is restricted due to the thickness of the cage faces and could potentially limit the success of the fusion. However, manufacturing the cage in two parts could potentially introduce unexpected stress concentrations at the contact areas. The various pores used in the cage design were effective at reducing the effective modulus while maintaining the strength of the structure. It is possible that the non-uniformity of the pores could introduce further unexpected issues during mechanical testing.

The most important result of this research was the feasibility and effectiveness of designing a cage with patient specific endplates. This type of orthopedic design has only recently begun to evolve in today's treatment practices. Utilizing the rapidly growing and improving 3D

printing industry for medical orthopedic practices would be beneficial to the entire medical community.

VII. FUTURE WORK

The vertebral bodies and a prototype of the cage have been manufactured through the use of a Stratasys Dimension and Stratasys Connex rapid prototyping machines respectively. The final product will be manufactured out of titanium (Ti-6Al-4V) using the DMLS process by C&A Tool. The vertebral bodies and the plastic prototype are shown in Figure 44 below.

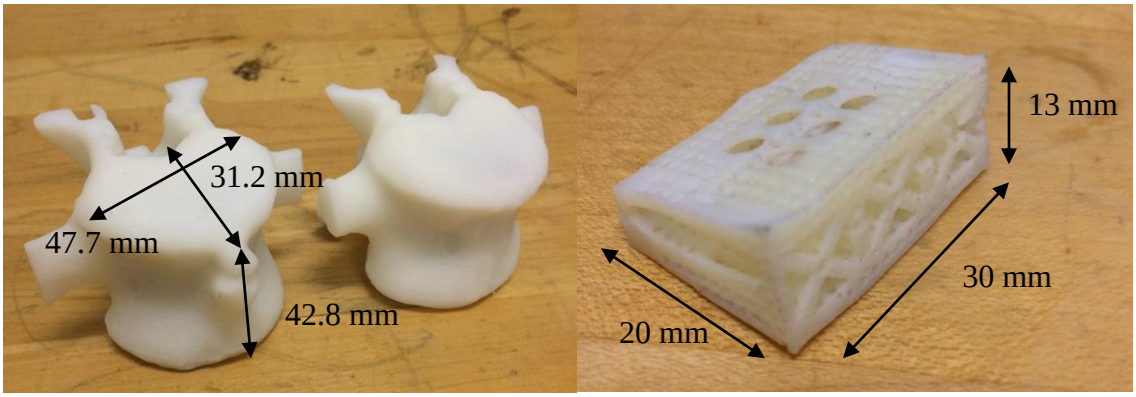

Figure 44: 3D printed vertebral bodies (Left) and 3D printed plastic cage prototype (Right).

The final cage will be viewed beneath a microscope to confirm the pore dimensions and separation distances. Once it has been confirmed that there are no major manufacturing inaccuracies such as disconnected or thin walls, it will then be possible to move on to mechanical testing. Using Delcrin thermoplastic blocks as replacements for actual vertebral bodies compressive testing can be done to determine the actual elastic modulus of the cage. It is important to check and compare the cage's actual material properties to those determined through the 3D modelling on SolidWorks. Further future work on this project would involve investigation into the possibility of patenting the patient-specific design as well as pursuing FDA

approval. Further investigation into the FDA approval of orthopedic implants manufactured using direct metal laser sintering is also necessary for the progression of the biomedical field.

REFERENCES

[1] "Lumbar Spinal Fusion Surgery." Spine-health. N.p., n.d. Web. 16 Nov. 2014.

[2] Douglas, Orndorff. " Force Transfer in the Spine." *Spinal Research Foundation* 7.2 (2012): 30-35. Web. 24 Sept. 2014.

[3] Marta Kurutz (2010). Finite Element Modelling of Human Lumbar Spine, Finite Element Analysis, David Moratal (Ed.), ISBN: 978-953-307-123-7, InTech

[4] "Spinal Fusion-OrthoInfo - AAOS." Spinal Fusion-OrthoInfo - AAOS. American Academy of Orthopedic Surgeons, June 2010. Web. 12 Nov. 2014.

[5] Ma, C. Benjamin. "Spinal Fusion: MedlinePlus Medical Encyclopedia." U.S National Library of Medicine. U.S. National Library of Medicine, 16 Apr. 2013. Web. 12 Nov. 2014.

[6] "Pennsylvania Spinal Cord Fusion Lawyers - Spinal Cord Fusion Lawyers in Pennsylvania." Console & Hollawell. N.p., n.d. Web. 22 Nov. 2014.

[7] "Posterior Lumbar Interbody Fusion." Orthopedic Topics. Eorthopod.com, n.d. Web. 22 Nov. 2014.

[8] Rifenbery, James. "Spine Exposure - Center for Minimally Invasive Surgery - Dr. James Rifenbery - Tacoma, WA." Spine Exposure - Center for Minimally Invasive Surgery - Dr. James Rifenbery - Tacoma, WA. Center for Minimally Invasive Surgery, n.d. Web.23 Nov. 2014.

[9] "ROI-T® TLIF." *LDR Latin America Productos Toraco-lumbar TLIF Jaula*. LDR, n.d. Web. 14 Mar. 2015.

[10] "XLIF Nuvasive." *American Institute of Minimally Invasive Surgery*. American Institute of Minimally Invasive Surgery, n.d. Web. 14 Mar. 2015.

[11] "Redondo ™ Anterior Lumbar Interbody Fusion System." Integra. Integra, n.d. Web. 22 Nov. 2014.

[12] "High Performance VICTREX PEEK Polymers - Victrex." Victrex. N.p., n.d. Web. 16 Nov. 2014.

[13] "Polyetheretherketone (PEEK) Material Properties :: MakeItFrom.com." Polyetheretherketone (PEEK) Material Properties :: MakeItFrom.com. N.p., n.d. Web. 22 Nov. 2014.

[14] "K2M Cayman Anterior Lumbar Plate." Life Healthcare. N.p., n.d. Web. 22 Nov. 2014.

[15] "Www.3ders.org." 3ders.org. N.p., 13 July 2014. Web. 22 Nov. 2014.

[16] "ROI-A® Oblique." LDR. N.p., n.d. Web. 22 Nov. 2014.

[17] Linder, Heather. "FDA Clears Renovis Surgical's Tesera Anterior Lumbar Interbody Fusion Cage." FDA Clears Renovis Surgical's Tesera Anterior Lumbar Interbody Fusion Cage. Becker's Spine Review, n.d. Web. 16 Nov. 2014.

[18] Peersman, G., R. Laskin, J. Davis, M. G. E. Peterson, and T. Richart. "Prolonged Operative Time Correlates with Increased Infection Rate After Total Knee Arthroplasty." HSS Journal 2.1 (2006): 70-72. Web.

[19] Kowalksi, Robert J., Lisa A. Ferrara, and Edward C. Benzel. "Medscape Log In." *Medscape Log In*. Medscape, 2001. Web. 22 Nov. 2014.

[20] "Describe the Differences between Primary and Secondary Bone Healing."- *OrthopaedicsOne Clerkship - OrthopaedicsOne*. OrthopedicsOne.com, 28 Nov. 2011. Web. 15 Nov. 2014.

[21] Broderick, J. Scott, and Timothy McHenry. "Home | Orthopaedic Trauma Association." *Home | Orthopaedic Trauma Association*. Orthopaedic Traumatic Association, Nov. 2005. Web. 22 Nov. 2014.
[22] Perren, Stephan M. "Evolution of the Internal Fixation of Long Bone Fractures: The Scientific Basis of Biological Internal Fixation: Choosing a New Balance between Stability and Biology." *The Journal of Bone and Joint Surgery* 84.8 (2002): 1093-110. Web.
[23] "Men's Weight Chart." *Mens Average Weight Chart*. N.p., n.d. Web. 16 Nov. 2014.
[24] Cappozzo, Aurelio. "Compressive Loads in the Lumbar Vertebral Column during Normal Level Walking." *Journal of Orthopaedic Research* 1.3 (1983): 292-301. Web.
[25] Bosco, Ruggero, Jeroen Beucken, and Sander Leeuwenburgh. "Surface Engineering for Bone Implants: A Trend from Passive to Active Surfaces." Coatings 2 (2012): 95-119.
[26] Eos, Source:. "EOSINT M Technology for Direct Metal Laser-Sintering (DMLS)." *EOSINT M Technology* (n.d.): n. pag. *3dimpuls.com*. EOS, 2007. Web. 22 Nov. 2014.
[27] Paolicelli, Alex. "The Optimization of Porosity and Pore Patterning for Patient-Specific Ti-6Al-4V Femur Implants." Thesis. Union College, 2014. Print.
[28] "Computed Tomography Radiology Reference Article." *Radiopaedia Blog RSS*. Radiopaedia.org, n.d. Web. 10 Mar. 2015.
[29] Zhou, S. H., I. D. Mccarthy, A. H. Mcgregor, R. R. H. Coombs, and S. P. F. Hughes. "Geometrical Dimensions of the Lower Lumbar Vertebrae - Analysis of Data from Digitised CT Images." European Spine Journal 9.3 (2000): 242-48. Web.
[30] "Tesera ALIF Cage System Sizes and Specs." Renovis Surgical. N.p., n.d. Web. 10 Mar. 2015.
[31] ": Products." Pezo®: Innovative Spinal Implants: Ulrich Medical USA®. N.p., n.d. Web. 10 Mar. 2015.

APPENDIX

Cube Porosity Variations:

1. 5x5, 1mm diameter pores in X,Y,Z directions. Corner pores are 1mm from closest edges. 2mm between pore centers.

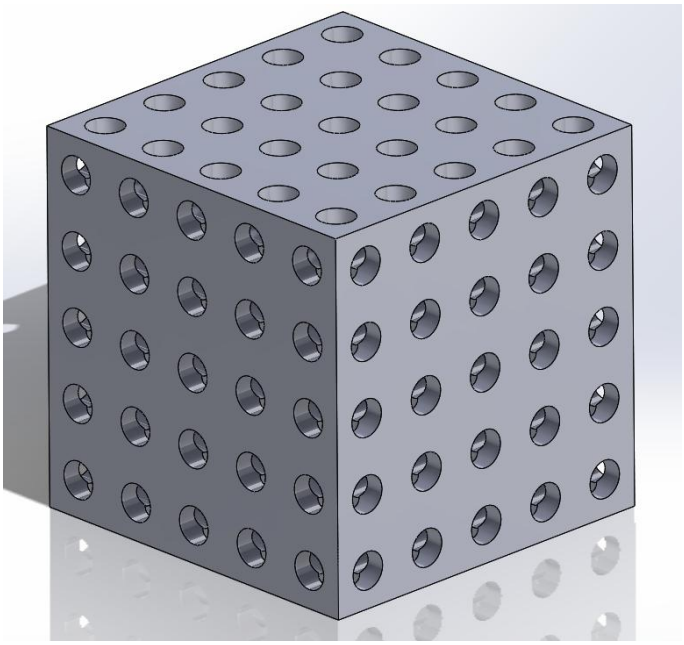

2. 9x9, 0.5mm diameter pores in X,Y,Z directions. Corner pores are 1mm from closest edges. 1mm between pore centers.

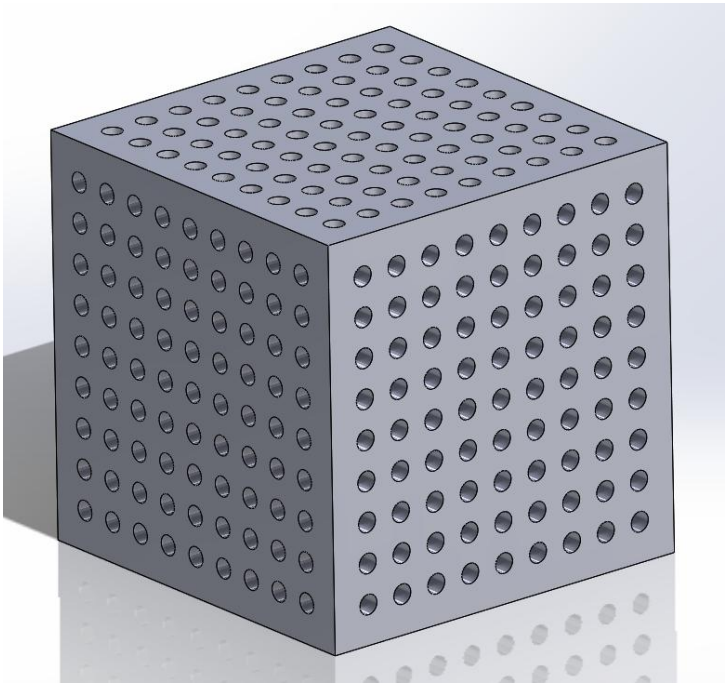

3. 4 Triangles in Z-Dir through all.

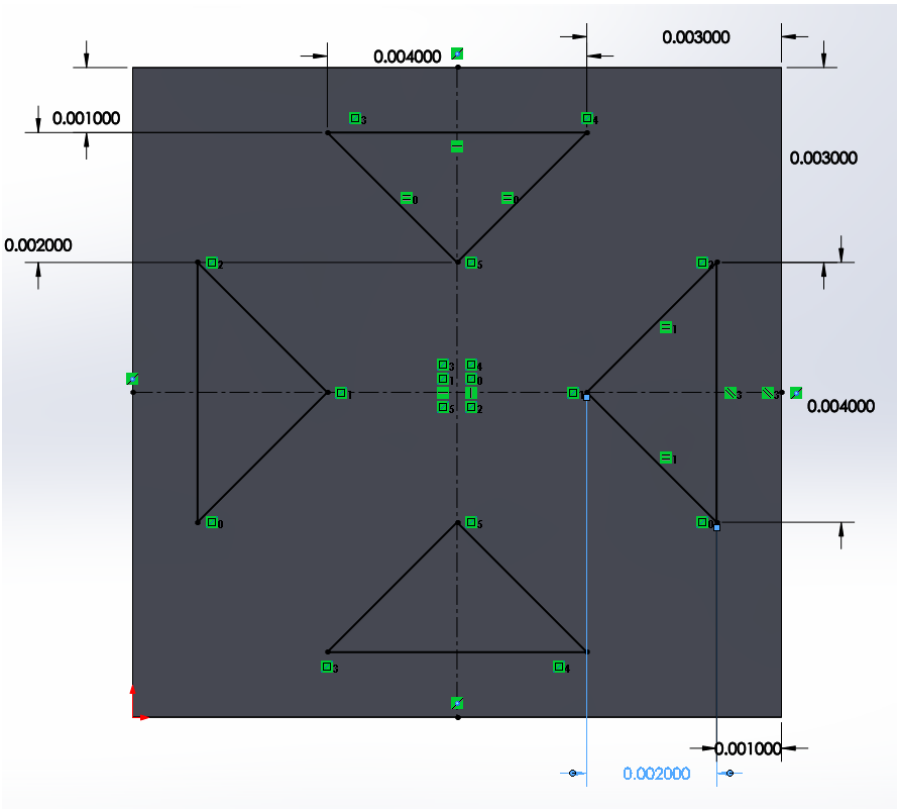

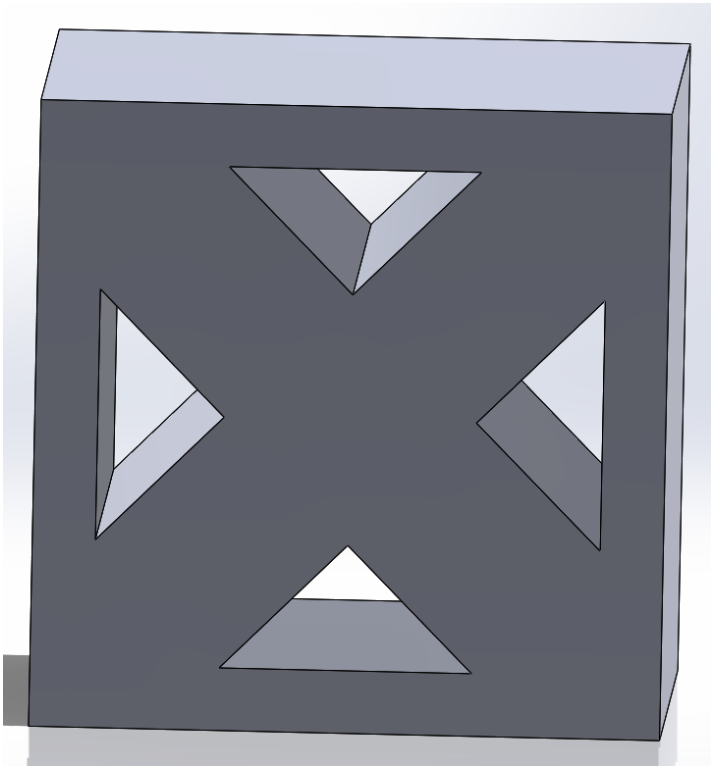

4. Same Triangles from [3] with pores from [1] in X-dir.

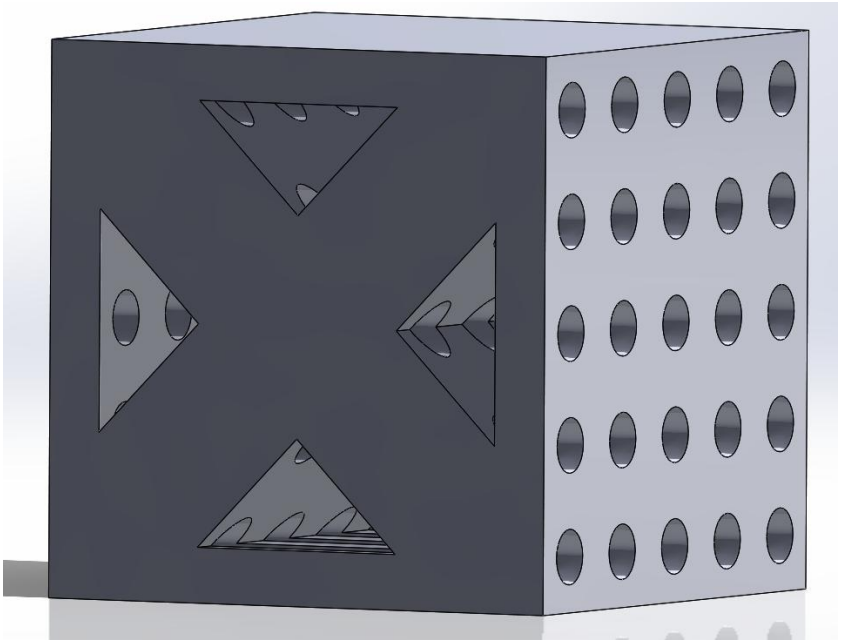

5. Same as [4] but with pores in X and Y-dir.

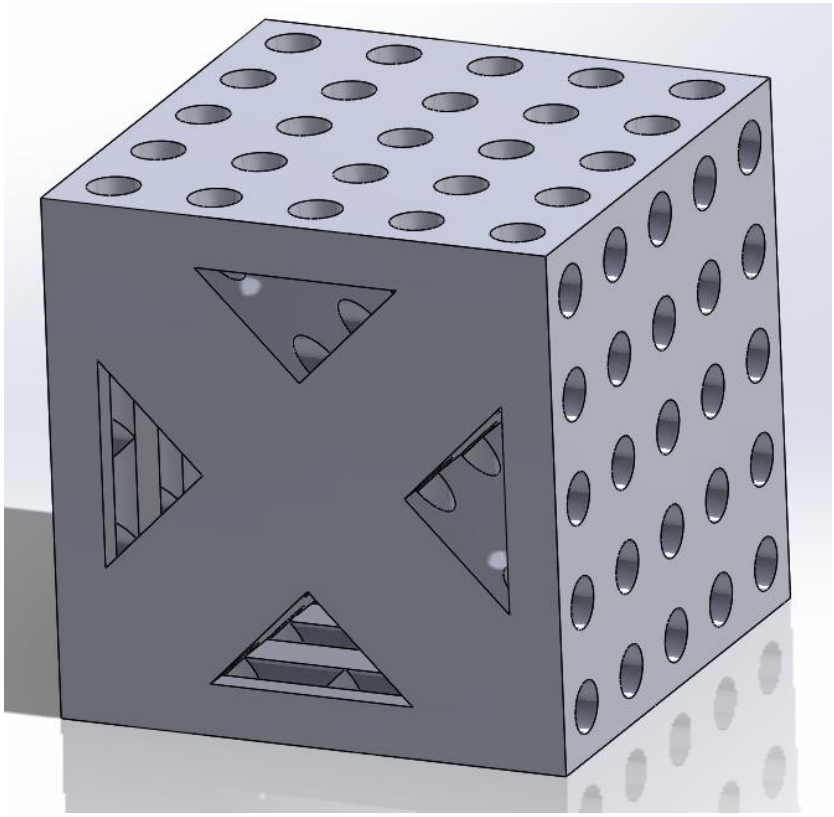

6. Same as [3] but with same dimension triangles creating a “cross” through X-dir as well.

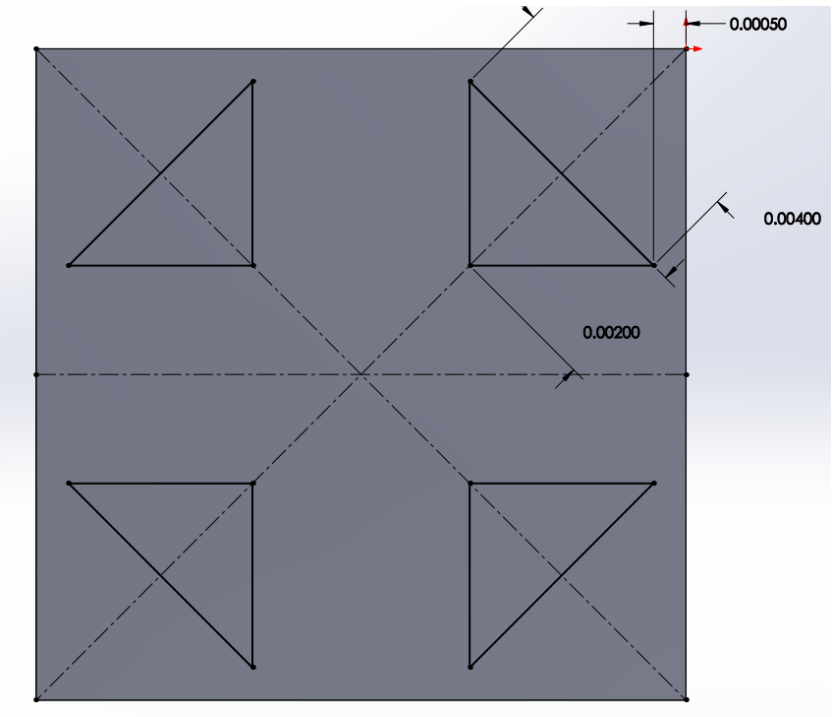

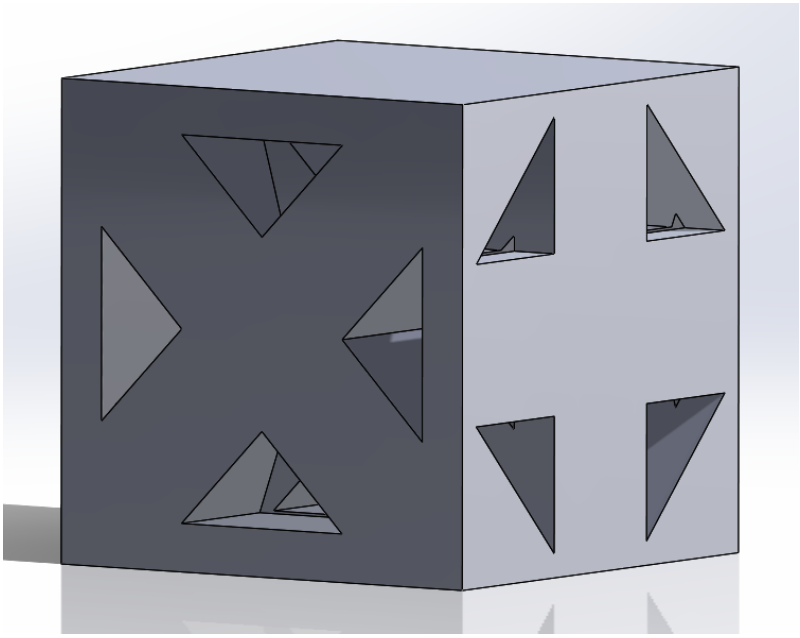

7. Same as [6] but with 5x5 1mm pores in Y-dir.

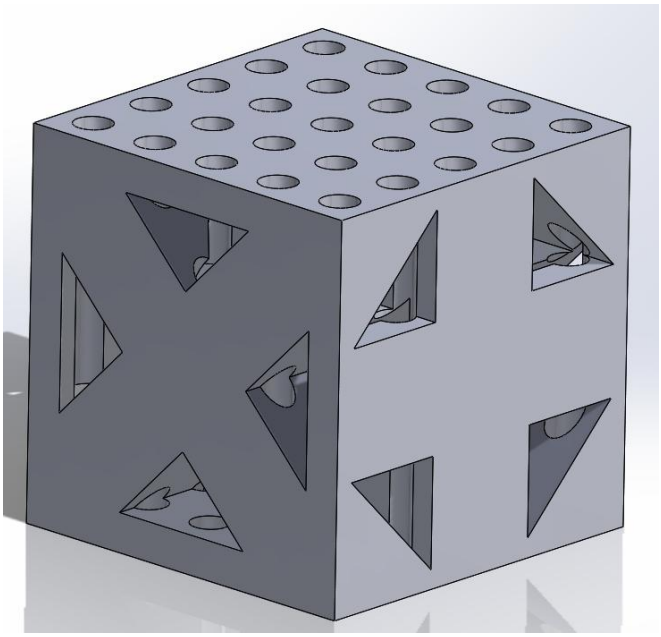

8. Same as [7] but with 10 0.5mm pores in each corner in the X-dir. Corner pores are 0.5mm from each edge and pores are 0.75mm from each other in the Y and Z-dir.

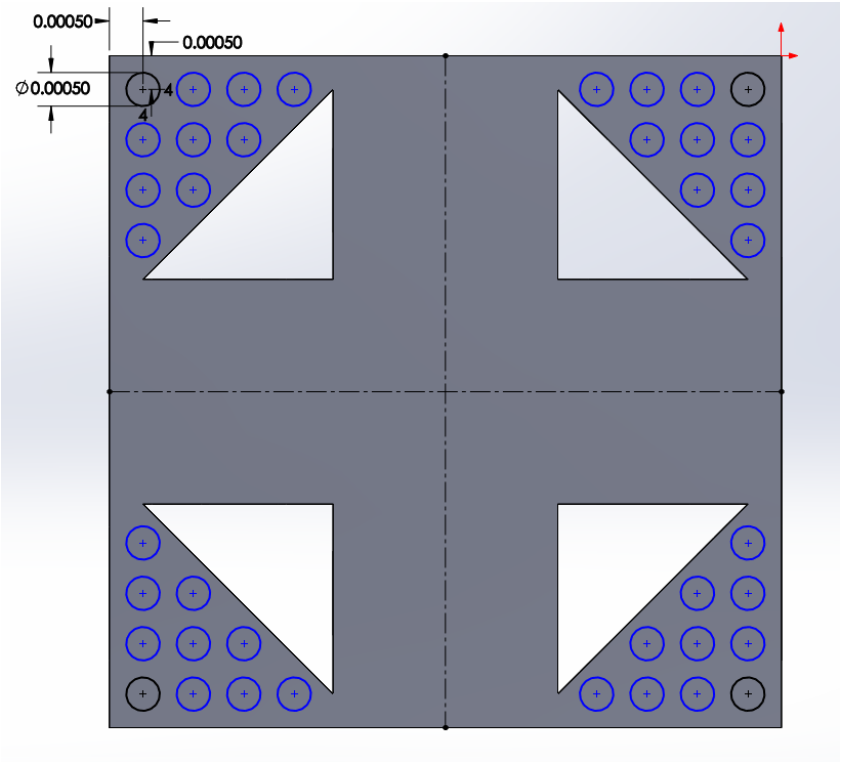

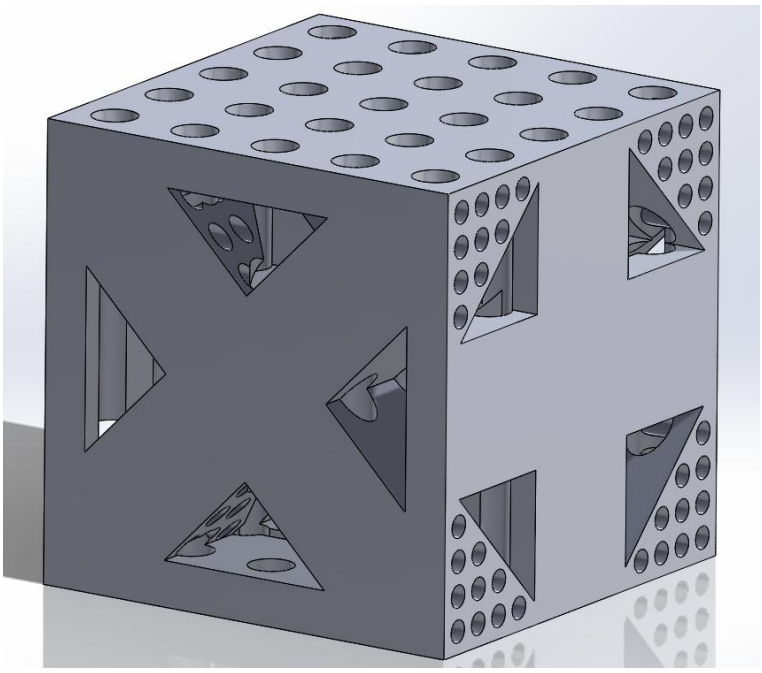

Iterations of [5]

9. 1mm pores through “X” with 1.3mm separations.

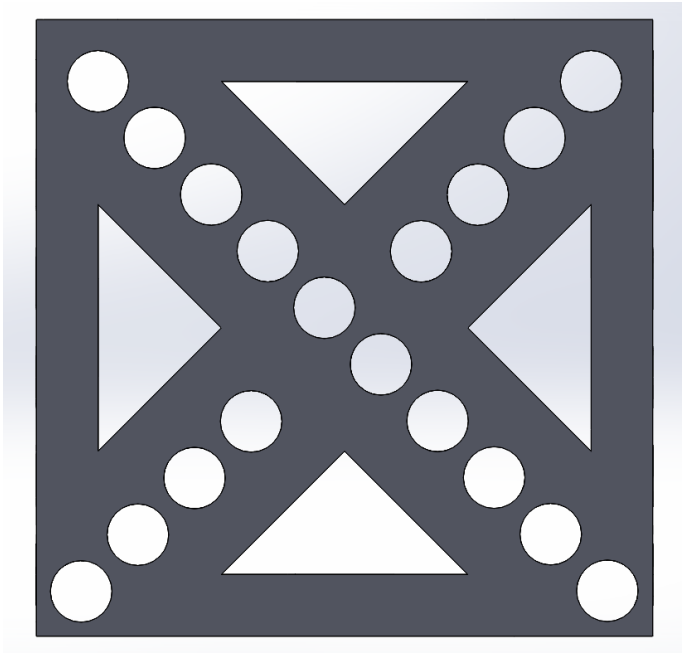

10. Same as [9] with 6x6 1mm pores with 1.6mm spacing.

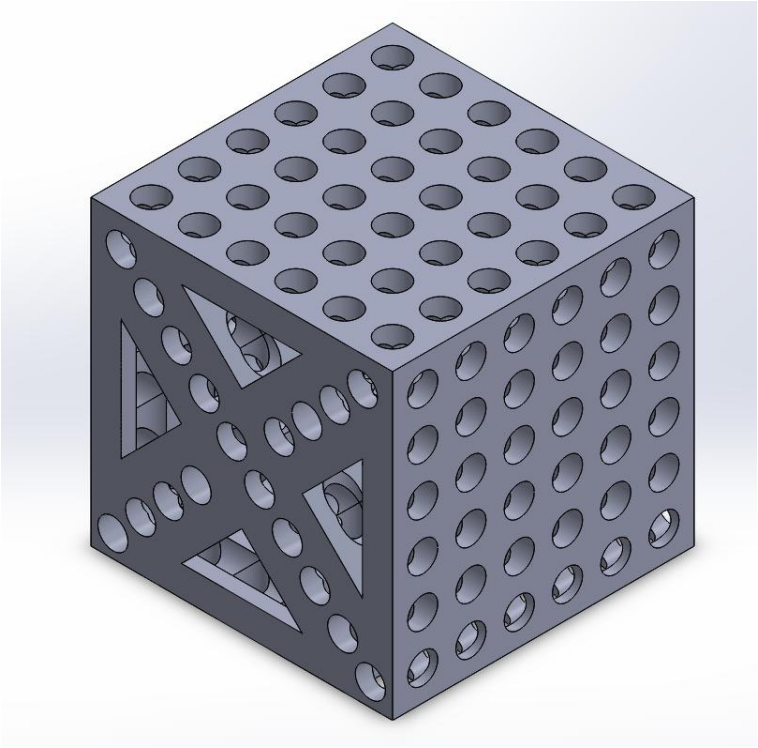

11. Same as [9] with 2 mm hole through center of ‘X’.

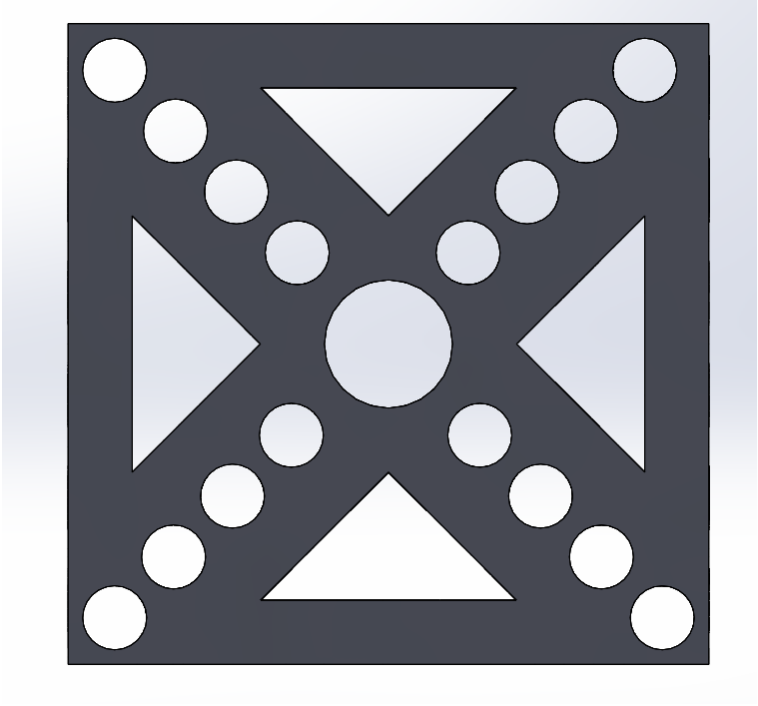

12. Same as [11] but with 9x9 0.75mm pores going through laterally.

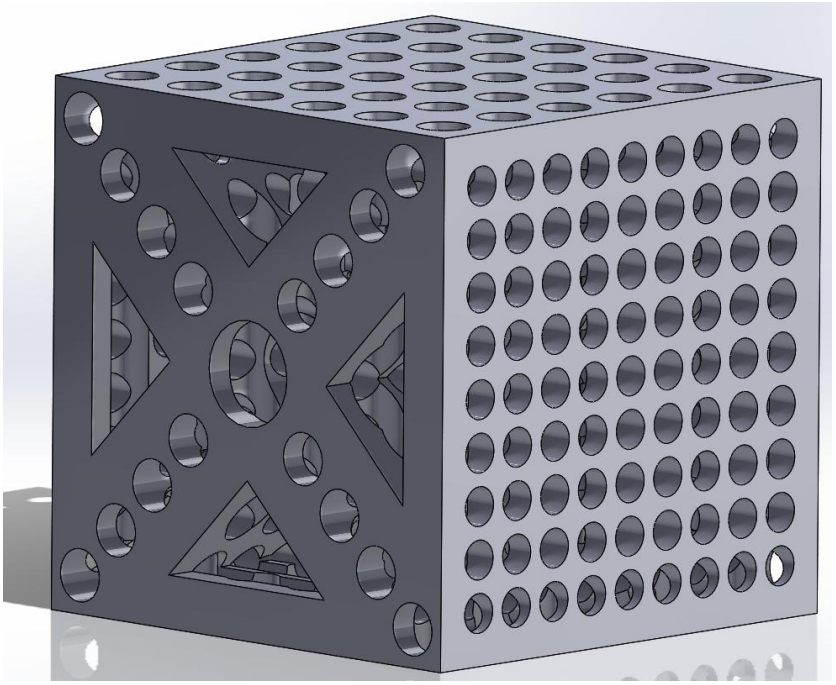

13. Same as [12] but with 2 2mm pores replacing 4 of the corner pores going through the ‘X’ and 0.5 mm pores instead of 0.75mm as shown below.

14. Same as [13] but with 6, 0.5mm pores 0.75mm apart instead of the 2mm pore in center of ‘X’.

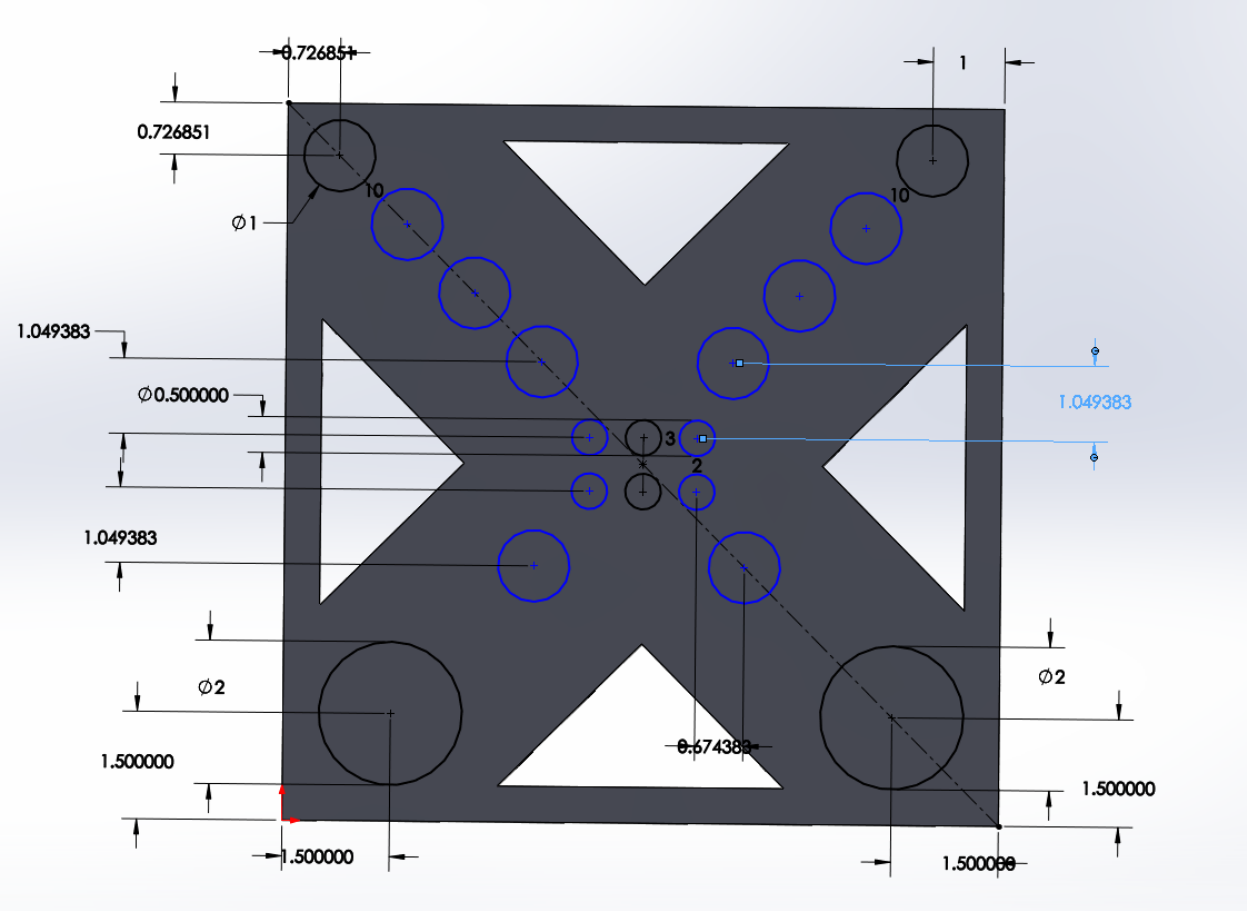

15. Same as [14] but with 81, .5 mm pores 1 mm apart on the top face.

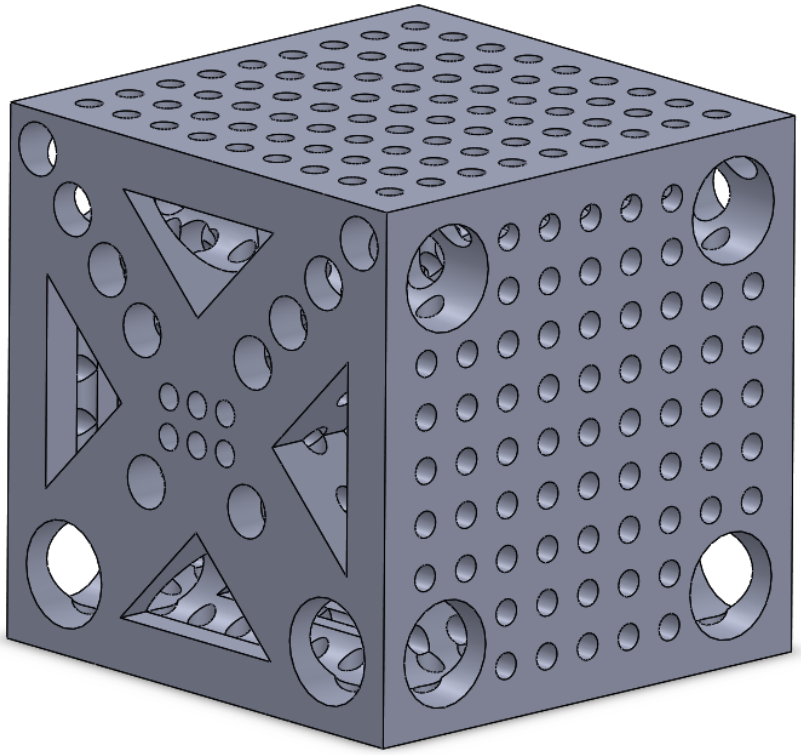

FEA Results for Iterations of [5]:

Iteration Number	Stress (MPa)	Deformation (mm)	Strain	Modulus (GPa)	Porosity (%)
0	30	0.0028626	0.00028626	104.7998323	0
1	30	0.0075054	0.00075054	39.97122072	41.23
5	30	0.012646	0.0012646	23.72291634	41.986
9	30	0.018864	0.0018864	15.90330789	51.986
10	30	0.022446	0.0022446	13.36541032	59.2033703
11	30	0.023057	0.0023057	13.01123303	60.186
12	30	0.037949	0.0037949	7.905346649	66.881
13	30	0.042536	0.0042536	7.052849351	62.159
14	30	0.041158	0.0041158	7.288983916	60.984
15	30	0.023122	0.0023122	12.97465617	52.8648